# DEVELOPMENT AND TESTING OF A STEERABLE CRUCIFORM PARACHUTE SYSTEM

A Thesis
IN
Mechanical Engineering

Presented to the Faculty of the University
of Missouri–Kansas City in partial fulfillment of
the requirements for the degree

MASTER OF SCIENCE

by
SHAWN MALACHY HERRINGTON

B. S., University of Missouri Kansas City, 2017

Kansas City, Missouri
2018

DEVELOPMENT AND TESTING OF A STEERABLE CRUCIFORM PARACHUTE SYSTEM

Shawn Malachy Herrington, Candidate for the Master of Science Degree

University of Missouri–Kansas City, 2018

## ABSTRACT

This thesis focuses on the development of a parachute payload system which is capable of precision aerial delivery yet only represents a modest cost increase over ballistic unguided systems. In order to develop such a system, first a canopy is selected. The canopy should be simple and inexpensive to make; in this case a cruciform canopy was selected because this design is material efficient and requires far less labor to manufacture compared to parafoil parachutes. Next some method of stabilizing that canopy during flight must be proposed. In this case, the system heading is to be stabilized via a single actuator by asymmetric deflection of the leading edge of one canopy panel. At this stage in the development, a controller must be designed and implemented which stabilizes the system in the proposed way. Outdoor flight testing is the gold standard of parachute testing methodology since it offers the most realistic flight conditions. However, the unmeasured wind disturbances encountered in outdoor flight testing can confound results

and interfere with repeatability of experiments.

The first experiment explained in this thesis revolves around the testing of a steerable cruciform parachute system using a vertical wind tunnel. The primary goal of the experiment was to develop a heading stabilizing controller. Additionally, a closed-loop system model was identified and a technique was developed for estimating canopy glide ratio (GR). The vertical wind tunnel testing methodology is far faster and less expensive than the outdoor flight testing which would be needed to accomplish the same goals.

After proving that a system can be steered via the proposed methodology, the next stage in the developing of a precision guided vehicle is to demonstrate that the stabilization technique is viable. This is accomplished in both outdoor flight testing and a simulation based on the closed-loop model identified earlier. Furthermore, the precision navigation potential of the system must be demonstrated; specifically, the system must be capable of arriving closer to the desired impact point on the ground than an unguided system dropped under the same conditions.

The work described in this thesis has advanced the development of the steerable cruciform parachute system beyond the point of simply being a feasibility demonstrator. The vertical wind tunnel experiments demonstrated that the system heading could be stabilized and subsequent navigation experiments demonstrated that the system outperforms an unguided system during real drops. The work done to compare the effectiveness of different navigation strategies in a simulated environment represents the beginning of the

next stage in the development of the parachute system. This next stage involves refinement and performance improvements of the existing platform through engineering design in order to advance the technical readiness level of the project.

APPROVAL PAGE

The faculty listed below, appointed by the Dean of the School of Computing and Engineering, have examined a thesis titled "Development and Testing of a Steerable Cruciform Parachute System," presented by Shawn Malachy Herrington, candidate for the Master of Science degree, and hereby certify that in their opinion it is worthy of acceptance.

Supervisory Committee

Travis Fields, Ph.D., Committee Chair
Department of Civil & Mechanical Engineering

Antonis Stylianou, Ph.D.
Department of Civil & Mechanical Engineering

Sarvenaz Sobhansarbandi, Ph.D.
Department of Civil & Mechanical Engineering

CONTENTS

ILLUSTRATIONS

# TABLES

ACKNOWLEDGEMENTS

Funding for the steerable cruciform project is provided primarily through the U.S. Army Natick Soldier Research, Development and Engineering Center (NSRDEC). The VST at NASA Langley Research Center was available through NASA EPSCOR. Thank you to Simeon Karnes who served as the PAVS laboratory intern during the summer of 2017 for making sure that all hardware and software was ready prior to the week of testing at the VST. Thank you to the staff at NASA Langley, Steve Riddick, Clinton Duncan, and Lee Pollard, for facilitating the VST experiments. Thank you to the staff at Yuma Proving Ground including Jose Ramirez, Randy Smith, Marc Christians and Ryan Tiaden. Finally, thank you to the members of the Parachute and Aerial Vehicles Systems Lab at UMKC including, Mohammed Alabsi, Jesse McDermott, Jeff Renzelman and Chris Tiemann, this would not have been possible without your help.

# CHAPTER 1

# INTRODUCTION

## 1.1 Precision Aerial Delivery

Resupply efforts in hard to reach locations often require the use of precision aerial delivery systems which can be deployed from high altitude and land within a specified distance of a predetermined impact point on the ground. For the past two decades many different solutions to the precision airdrop problem have been proposed. Several techniques including pneumatic muscle actuators [1–3], reversible reefing [4, 5] and optimized drogue-to-main transition timing [6–9] have focused on improving the impact point accuracy of inexpensive circular canopies. The impact point accuracy and disturbance rejection of these methods is limited by the narrow translational capabilities of circular canopies. Other methods have focused on ram-air parafoil systems due to their greater glide capabilities [10–16]. Recent efforts have demonstrated the potential utilization of cruciform canopies as a low-cost semi-precision delivery platform [17].

While parafoil systems can achieve highly favorable impact point accuracy, their relatively high cost may be discourage use in some situations. All solutions to the precision airdrop problem strike a balance between impact point accuracy and system cost. With current solutions, planners of resupply missions could be forced to choose affordability over accuracy or vice versa. The steerable cruciform system fills the gap between existing technologies by delivering acceptable impact point accuracy with low associated

operational costs. The steerable cruciform system (dubbed SnowflakeX) requires only a single actuator to steer and glide the vehicle. Steering and glide capabilities are achieved through asymmetric canopy deformation, similar to the methods used in the Affordable Guided Airdrop System (AGAS) [1–3].

## 1.2 Steerable Cruciform Parachute System

The steerable cruciform is a parachute system consisting of a cruciform canopy trimmed for glide in a manner similar to the techninques shown in [18] in which the canopy panels are asymmetrically deformed to generate horizontal glide. The concept requires only a single actuator to stabilize the canopy heading. Unlike unguided systems which by definition are completely susceptible to wind drift, the steerable cruciform system seeks to achieve sufficient impact point accuracy to enable drops to be conducted from greater than $10\,000\,\mathrm{ft}$ [$3048\,\mathrm{m}$] altitude above ground level (AGL) in order to significantly improve aircraft safety [17].

The steerable cruciform system utilize a hybrid navigation strategy which relies on a wind prediction to drop the system at the calculated aerial release point (CARP) and steer the system along a reference trajectory [17, 19]. The reference trajectory represents the ballistic trajectory that would need to be followed by a similar but unguided system in order to arrive exactly at the impact point if the winds were known perfectly. The navigation algorithm points the system toward successive altitude-dependent waypoints. Errors in landing location occur because of differences between the predicted and actual wind conditions.

The system evaluated in this study has a descent rate of approximately $22\,\mathrm{ft/s}$ [$6.8\,\mathrm{m/s}$], and the system can only penetrate winds up to $8.0\,\mathrm{ft/s}$ [$2.5\,\mathrm{m/s}$]. Wind penetration is defined as the ability of the system to steer directly into wind of a given speed and still move forward in terms of the ground track. The system works in conditions where the wind speed is well in excess of $8.0\,\mathrm{ft/s}$ [$2.5\,\mathrm{m/s}$], but since it cannot make forward progress into a strong wind, it relies on an accurate prediction of winds in the drop zone to develop an intelligent path to the impact point. The system is designed such that only minor corrections to the reference trajectory are required during descent to achieve significantly improved landing accuracy over an uncontrolled system. When the wind forecast is accurate, the steerable cruciform system offers substantially improved impact point accuracy compared to unguided ballistic systems [17].

The steerable cruciform concept is built upon preliminary work which investigated the navigational potential of cruciform canopies [18, 20]. In the 2003 study, Potvin *et. al.* evaluated canopies attached to human-sized payload from an aircraft at $1000$ to $2000\,\mathrm{ft}$ ($305$ to $610\,\mathrm{m}$) AGL with a typical flight lasting $1$ to $2\,\mathrm{min}$ [18]. Tests were conducted with both static deformation and remotely controlled deformations. Work done by Fields and Yakimenko dropping a $12\,\mathrm{lbf}$ ($53\,\mathrm{N}$) payload from $1600$ to $2000\,\mathrm{ft}$ ($488$ to $610\,\mathrm{m}$) AGL resulted in similar total flight times [17]. Data from flight tests was used to create a simulation to study navigation performance with respect to quality of wind prediction [19]. The short duration of descent during flight tests presented a challenge in terms of conducting experiments to develop an autonomous heading stabilization controller.

Two navigation schemes have been evaluated in outdoor flight testing. The first of these schemes is known as persistent point-toward-target navigation. This type of strategy makes sense for an autonomous vehicle navigating in a flat planar space free of obstacles. By always commanding the system heading to point from the current position to the target, perfect impact point accuracy can be guaranteed as long as the vehicle can turn in place. SnowflakeX cannot turn in place and is the desired impact point is represented by a point in three dimensional space rather than a point on a plane. However, the point-toward-target navigation strategy does not require any prior knowledge about the wind conditions in the drop zone. In fact, if the wind velocities are sufficiently low and the system is dropped with a reasonable offset from the impact point, then the system should arrive at the target zone with improved accuracy over a ballistic system dropped from the same place. In general, solutions to the precision airdrop problem should make use of an estimate of the wind conditions in the drop zone since the wind conditions can easily overpower the navigational authority of the parachute. This is especially true for SnowflakeX which according to the low GR can only penetrate a prevailing wind of about $8\,\mathrm{ft/s}$ [$2.5\,\mathrm{m/s}$].

The second navigation scheme is known as waypoint navigation. For this strategy a trajectory is generated which represents the ballistic trajectory which should be taken by a similar system to SnowflakeX but which has no guidance capabilities, in order to arrive at the desired impact point perfectly if the winds in the drop zone have not changed since the wind information was recorded. At the top of this ballistic trajectory is the location where the drop should occur which is known as the computed aerial release point

(CARP). The continuous ballistic trajectory is sampled at uniform altitude intervals in order to develop the altitude dependent waypoints which will be loaded on the aerial guidance unit (AGU). During a drop, the system heading is commanded to point toward the current waypoint based on the current altitude. When the subsequent altitude level is reached, the system receives a new waypoint which the system heading will subsequently be commanded to point toward. This procedure is repeated until the final altitude layer is reached at which point the current waypoint is the same as the desired impact point on the ground. The waypoint navigation scheme demonstrates improved impact point accuracy if the wind prediction for the drop zone is reasonably good.

## 1.3 Contributions

The main contributions of this work are as follows:

- **A solution is proposed to the precision airdrop problem which takes advantage of an inexpensive cruciform canopy design**
- **A control strategy is proposed and a controller is designed using a vertical wind tunnel**
- **The guidance capabilities are demonstrated in flight testing**
- **Advanced guidance strategies which enhance the impact point accuracy are vetted using a numerical simulation**

## 1.4 Thesis Organization

This thesis is organized as follows. First a literature review is presented with overviews of historical work and the state of the art of several important topics. These topics are parachute testing methodologies, the history of the NASA 20 ft. Vertical Spin Tunnel, parachute system navigation and control strategies and trajectory planning and tracking algorithms. Next a detailed accounting of the experiments conducted at the vertical wind tunnel is presented. This section includes information about the test setup including the wind tunnel itself and the parachute system hardware using. Experimental methods and results are then provided followed by conclusions specific to the experiment. Next an accounting of various experiments to investigate the navigational potential of the SnowflakeX system is presented. In this section, flight test results are presented followed by simulation results. An explanation of the limitation of the simulation as well as the specific methodology used is included. The end of this thesis contains overall conclusions related to this work. These overall conclusions relate the information provided in the previous section to the precision aerial delivery problem. Additionally, the conclusions suggest potential future work which builds on the findings of this work.

# CHAPTER 2

# LITERATURE REVIEW

## 2.1 Parachute Testing Methods

Prior to the current state of the art in computation fluid dynamics which allows complex aerodynamic interactions to be studied in simulation, other methods were developed for physical testing of parachute systems without the hassle and expense of flight testing. The now demolished whirl tower constructed at Naval Air Facility El Centro, in El Centro, CA was erected to study and evaluate parachute deployment characteristics [21]. The tower consisted of a central spinning tower crane to which an aerodynamic gondola was attached. Parachute systems under test were attached to the gondola with a radio controlled release system. Electric motors drove the spinning motion of the central crane and the gondola swung out from the crane on a cable tracing a $350\,\mathrm{ft}$ [$107\,\mathrm{m}$] diameter circle more than $120\,\mathrm{ft}$ [$37\,\mathrm{m}$] above the ground. Once the system was up to speed, the radio controlled release system was activated and the parachutes systems and attached payloads would fly outward from the gondola.

Recomendations from a study published on the instability of the gondola system [22] drove improvements which resulted in a maximum simulated deployment speed of $400\,\mathrm{kts}$[21]. A technical report on the tower claims that equipment in the gondola was subject to upwards of 80g acceleration when the tower was at full rotational speed[21].

One study used the tower to study effects of storage on the permeability of flat

circular canopies [23]. In this study, parachutes originally constructed and tested $12\,\mathrm{yr}$ prior were subjected to varying deployment speeds using the whirl tower. The results of this study were important in boosting the understanding of the effects of long-term storage and line entanglement on parachute system characteristics [23].

One study used the tower to study effects of storage on the permeability and by extension the opening characteristics of flat circular canopies [23]. In this study, parachutes originally constructed and tested $12\,\mathrm{yr}$ prior were subjected to varying deployment speeds using the whirl tower. Intentionally mis-rigged and tangled parachutes were tested to ensure that the findings would be applicable under real world conditions [23]. The results of this study were important in boosting the understanding of the effects of long-term storage and line entanglement on parachute system characteristics [23].

Another historically common method for testing parachute systems has been to drop the parachute systems from a crane. This allows the free flight dynamics to be studied in a much more controlled manner than deploying from an aircraft. A 1967 study [24] investigated scale factors for the construction of parachute models using experimental data collected from crane drops. In the study, the parachutes under test were initially held in a "forced-reefed" condition where the canopy is affixed to a rigid metal hoop [24]. The testing apparatus then allowed the canopy to openly freely once dropped. This study presents a good example of one of the primary disadvantages of crane testing. The usefulness of a crane drop experiment is strongly tied to the height of the crane.

A series of crane drop experiments was used by the military during testing for age of life extension for the T10 main parachute, harness and reserve chute [25, 26]. In these

experiments, the crane drop was used to study opening characteristics only, meaning that a small crane could be used. For an age of life extension study, a large quantity of data must be collected in order to sufficiently prove that the findings are applicable. For this reason, a crane drop was selected in this case to allow data to be rapidly collected, thereby speeding up the process of experimental validation [25].

More recently, testing of a decelerator system for a private space capsule was conducted from a $360\,\mathrm{ft}$ [$110\,\mathrm{m}$] tall gantry crane at an industrial park in Denmark [27]. Even though this crane is exceptionally tall, the height was sufficient only to study the initial canopy deployment and reefing [27]. The deployment process and reefing performance of different slider configurations was studied by dropping the parachute system from a deployment bag suspended from the crane [28].

Various studies have used model aircraft or other UAV to conduct flight testing at a significantly reduced cost compared to hiring a manned aircraft [17, 19, 29]. Experimental data collected from alternative methods may still be subject to many of the other challenges associated with flight testing. Airdrops from whirl towers, cranes and UAV are still subject to unknown winds. Additionally, these methods may be subject to long reset time associated with the experimental apparatus as well as possible lost time due to difficulty in recovering the parachute system itself.

In 2013, a novel method for parachute load testing was presented in [30]. In this study, a parachute attached to a rocket sled, was dropped from a helicopter prior to firing the rockets in order to simulate the shock loading which would be experienced during deployment in a martian atmosphere [30]. This methodology is meant as an alternative

to dragging parachutes through viscous fluids (water) and firing payloads from cannons which are more traditional methods of load testing large canopies [30].

Vertical wind tunnel testing itself is not a new testing methodology, but parachute testing at such sites has been limited. The primary impediment to VST testing is finding a location which is both sufficiently large enough to accommodate the system under investigation and also willing to allow the facility to be used for research. A group of researchers was able to use a commercial indoor skydiving facility to study the stability characteristics of a model of a proposed private space capsule in 2012 [31]. The results of this study helped inform design changes to the vehicle in order to maintain stability during exit and re-entry of earth's atmosphere. This testing methodology is not unlike the testing which was conducted by NASA on the longitudinal stability of the Mercury Space Capsule [32].

Various studies have been conducted which use wind tunnel testing [12], computational fluid dynamics [33] or a combination of the two [11, 20] to study the glide characteristics of parachute systems. While alternative strategies have attempted to capitalize on the the lack of glide characteristics of flat circular canopies [4, 5], most parachute systems which have been designed for precision guidance make use of a relatively large glide ratio in order to achieve the required horizontal offsets and navigational authority [11, 12, 14].

## 2.2 History of the NASA 20 ft. Vertical Spin Tunnel

Completed in 1941, the 20 ft. Vertical Spin Tunnel (VST) at NASA Langley Research Center in Hampton, VA is the largest vertical research wind tunnel in the western

hemisphere. Originally designed and built to study the spin and recovery motion of free flying aircraft models, the VST has been used for various studies over the years. A 1997 report details a preliminary investigation conducted by Lockheed Martin into the feasibility of a jet fighter aircraft with no vertical stabilizing surfaces [34]. The results from this preliminary study conducted with minimal investment at the VST was to determine that eliminating vertical tail surfaces from a fighter aircraft could signfigantly degrade spin recovery characteristics for certain spin modes [34]. An early technical report indicates that the VST has been in continuous use since it was finished in 1941 and goes on to give examples and explain the methods which are generally used to study aircraft spin behavior at the VST [35]. The tunnel itself comprises a $20\mathrm{ft}$ [$6.1\mathrm{m}$] diameter by $25\mathrm{ft}$ [$7.6\mathrm{m}$] tall test section and is capable of a maximum wind velocity of $85\mathrm{ft/s}$ [$26.0\mathrm{m/s}$].

## 2.3 Parachute System Control Strategies

Traditionally, parachute systems are steered by asymmetrically deflecting some part of the canopy. Parafoil systems in particular can be thought of behaving in a manner similar to a rigid wing when inflated during steady flight. By this analogy, brake deflection to steer parafoils can be thought of as similar to the way an aircraft is steered using the rudder. For other types of parachutes, other methods of steering have been proposed. These methods range in complexity from attempting to give circular canopies gliding and steering characteristics, to modifying the descent rate during flight to simply timing the transition from drogue-to-main parachute in order to improve impact point accuracy for ballistic drops. These techniques are discussed in detail below.

## 2.4 Trajectory Planning and Tracking Strategies

### 2.4.1 General Trajectory Planning

There is much research focused on the development of efficient methods for planning and tracking reference trajectories for all types of vehicles. Trajectory planning for unmanned aerial vehicles (UAV) has focused on the problem of tracking non-linear reference trajectories as well as building a trajectory tracking controller which augments a commercially available autopilot controller [36–38]. Cues from the gain scheduling approach are applied in order to create a series of easy to analyze linear-time-invariant plants which are exploited to design an trajectory planner capable of maintaining constant airspeed while tracking an arbitrary inertial trajectory [36]. Further work into fixed-wing and rotor-craft UAV concerns augmenting commerical-off-the-shelf flight controllers using $\mathcal{L}_1$ adaptive control then an outer loop controller is added which is capable of non-linear trajectory tracking while simaltaneously meeting constrains required to avoid collisions with other (UAV) [37]. Building on this work, path following for multiple UAV is designed which can explicitly handle a wide range of maneuvers speeds and the strategy is demonstrated to outperform traditional waypoint navigation strategies [38].

Model predictive control (MPC) has seen widespread use in trajectory planning and tracking algorithms because these techniques can inherently handle constrains [39, 40]. MPC forms a robust technique for trajectory tracking due to the ability of a well designed algorithm to deal with non-linear or non-continuous paths without first linearizing or approximating a smooth path through similar waypoints [41]. The wide applicability of MPC has seen use in many types of UAV from aerodynamic vehicles [36–38, 42–46]

to water-based vehicles [39] to ground vehicles [41].

### 2.4.2 Parafoil Trajectory Planning and Tracking

The challenges associated with improving the impact point accuracy of an underactuated aerodynamic decelerator vehicle are not new. Designers of guided ram-air parafoil systems have been investigating trajectory generation and tracking schemes which improve impact point accuracy [16, 43, 45, 47–50]. An overview of recorded parafoil trajectories indicates that most system use a multi-stage trajectory [16]. The terminal guidance phase is the most critical to the impact point accuracy of these systems since the low altitude leave no room for error if the final turn or approach is timed incorrectly.

Various trajectory planning and tracking algorithm improvements have been proposed specifically for parafoils. Gauss pseudospectral methods [48], model predictive controllers [42, 43, 45] have been developed and demonstrated to exhibit improved performance in simulations. Parafoil systems have been augmented with additional degrees-of-freedom (DOF) in order to affect glide slope during descent [50]. This technique outperforms traditional methods and the performance improvement increases with a rise in the uncertainty in the wind prediction in the drop zone [50].

The development of descent rate control (DRC) sought to control the trajectory of a parachute with authority over the descent rate as the single degree-of-freedom (DOF) for control [4, 5]. While the problem of navigating parafoil systems is commonly cast in terms of a single DOF, that degree of freedom is usually the yaw angle defined in the fixed

earth frame. For DRC, the desired landing area is described by a line rather than a point which is typically used for other systems. Simulations demonstrate that DRC outperforms unguided systems only when the wind is known reasonably well. For situations where the wind conditions in the drop zone are not well known, there is very little advantage to using descent rate control compared to an unguided drop [4, 5].

# CHAPTER 3

# VERTICAL WIND TUNNEL EXPERIMENT

This chapter discusses experiments conducted to develop a stabilizing controller using a vertical wind tunnel facility. The use of this facility allowed a highly efficient and data rich experimental program to be conducted without the confounding of external wind disturbances which are unavoidable in outdoor flight testing. The experiment was successful and the results demonstrate that a heading stabilizing controller was developed. Additionally, a dynamic model relating the input desired heading to the measured heading in the earth frame as well as a dynamic model relating the constrained pitching motion in the vertical wind tunnel to the expected glide performance in free flight was developed.

This chapter begins with a discussion of the vertical wind tunnel facility itself. Next the test article itself is presented followed by information about a photogrammetric experiment in order to characterize relative yaw motion between the payload and canopy. Next the methodology used for each of three distinct experiments is explained followed by the results of those experiments. Concluding remarks are provided which explain the importance of the experimental program presented here in terms of impact on the larger aerodynamic community. Potential future uses of the experimental program are also discussed.

## 3.1 NASA 20 ft. Vertical Spin Tunnel

Completed in 1941, the 20 ft. Vertical Spin Tunnel (VST) at NASA Langley Research Center in Hampton, VA is the largest research vertical wind tunnel in the western hemisphere. Originally designed and built to study the spin and recovery motion of free flying aircraft models [51], the VST has been used for many studies over the years. For example, a 1997 report details a preliminary investigation conducted by Lockheed Martin into the feasibility of a jet fighter aircraft with no vertical stabilizing surfaces [34]. The tunnel itself comprises a $20\mathrm{ft}$ [$6.1\mathrm{m}$] diameter by $25\mathrm{ft}$ [$7.6\mathrm{m}$] tall test section and is capable of a maximum wind velocity of $85\mathrm{ft/s}$ [$26.0\mathrm{m/s}$]. A photograph of the outside and a cutaway schematic representing the inside of the VST are shown in Figures 1a and 1b respectively.

The NASA Vertical Spin Tunnel is a closed-loop annular return type tunnel in which the air in the test section is continuously recirculated through the return passages which form a ring around the inner test section and the surrounding personnel area. The tunnel is powered by a three-blade axial fan in the roof of the tunnel. Since the tunnel was built to study spin characteristics of aircraft and not necessarily precision aerodynamic characterization, the potential for the fan to induce a spinning flow is seen as a feature rather than a detrimental characteristic. Therefore, effects of any potential flow bias should be accounted for when testing in the VST. The floor of the vertical wind tunnel is made up of a metal honeycomb structure which offers some flow straightening and provides a place for personnel to stand as well as a hard point for anchoring systems in the test section. A safety net at the bottom of the wind tunnel prevents items in the test

section from falling onto the honeycomb. The upper safety net shown in Figure 1b was removed during the steerable cruciform experiments in order to accommodate the large canopy.

(a) Exterior view of vertical spin tunnel building.

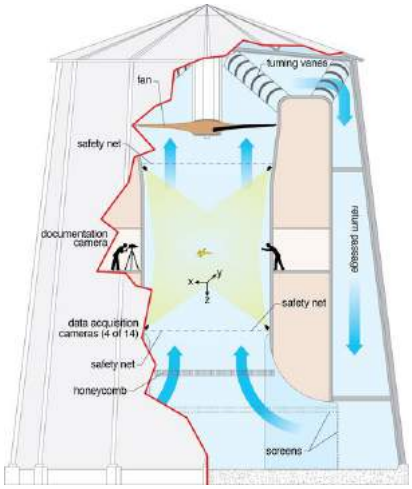


(b) Cutaway schematic of vertical wind tunnel

Figure 1: NASA 20ft. vertical wind tunnel

### 3.2 Test Setup

This section describes the specific configuration of the steerable cruciform parachute system tested along with the test set-up and measurement procedures as established for experiments in the vertical wind tunnel. A photo of the test article (payload) is shown in Figure 2. The steerable cruciform system payload contains the aerial guidance unit (AGU), actuators, batteries, and ballast weight. All of the internal components are installed inside of a Pelican 1200 case to improve the survivability of outdoor testing.

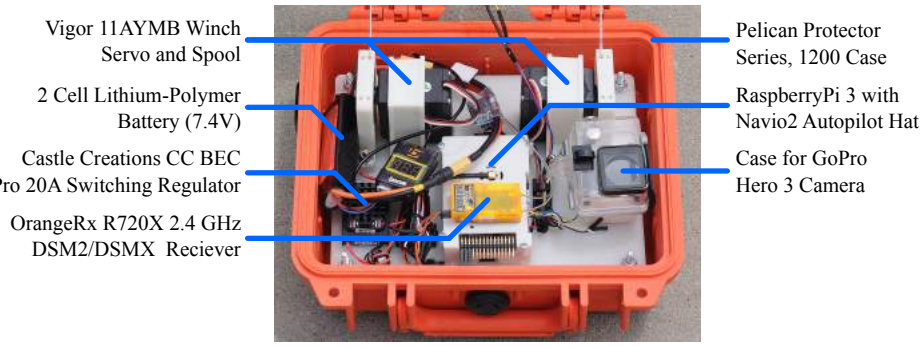


Figure 2: Test article (system payload).

### 3.2.1 Test Article

The AGU for the system consists of a RaspberryPi3 with a Navio2 autopilot hat. The Navio2 provides sensor information from dual 9 degree-of-freedom (DOF) intertial measurement units (IMU) to the RaspberryPi. The autopilot software, which is written in C++, writes all of the raw sensor information to a log file at $100\,\mathrm{Hz}$. The control calculations are also performed at $100\,\mathrm{Hz}$ while the attitude estimate is provided by a Madgwick Filter [52] algorithm operating at $300\,\mathrm{Hz}$. To facilitate the efficient collection of experimental data, the system can be activated remotely via radio control (RC) transmitter so that a remote operator can start and stop multiple experimental trials without interacting with a computer.

For the vertical wind tunnel experiments two actuators were installed in the payload. For any given experiment, only one actuator was being used dynamically to adjust the length of the dynamic line ($\delta_d$) while the other actuator was used to hold the static line at a fixed length called the static length ($\delta_s$). Having the capability to steer the system using an actuator on either side allowed the natural spin tendency of the tunnel to

be quantified according to the difference between the heading rate dynamics according to which direction the system was spinning.

Conceptually, when both the static length and the dynamic length are equal to the nominal length ($\delta_n$) as shown in Figure 3a, the canopy is uniformly inflated and exhibits no glide or spin behavior. When the static length and dynamic length are equal but both are less than the nominal length as shown in Figure 3b, the canopy glides toward the deflected suspension lines with a glide ratio of $1:0.25$ to $1:0.50$ [17, 18]. If the dynamic line length is shorter than the nominal length but the static line length is equal to the nominal line length as shown in Figure 3c, then the canopy will spin toward the side of the shortened dynamic line. A schematic of the cruciform canopy with the critical dimensions is shown in Figure 4b.

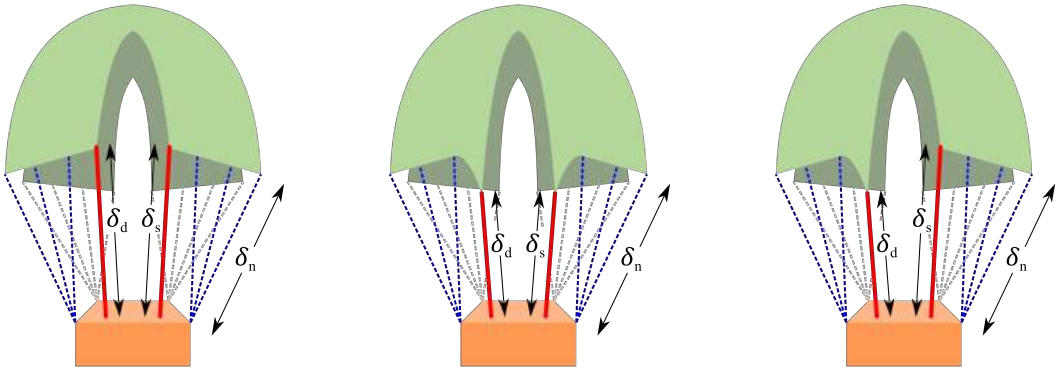


(a) Neutral rigging. (b) Rigging for glide. (c) Rigging for spin.

Figure 3: Steerable cruciform parachute system and rigging configurations.

The compass on the Navio2 was used for determination of the heading angle in the fixed earth frame. To calibrate, the translational bias representing the 3-dimensional offsets (hard-iron) as well as the full rotation and scaling matrix (soft-iron) calibration were

(a) Cruciform dimensions.

| Quantity | Big Canopy in (cm) | | Small Canopy in (cm) | |
|---|---|---|---|---|
| $l_1$ | 41 | (104) | 22 | (56) |
| $l_2$ | 28 | (71) | 22 | (56) |
| $\delta_n$ | 108 | (274) | 57 | (145) |
| $\delta_{d,neut}$ | 101.5 | (258) | 52 | (132) |
| $\delta_{s,min}$ | 92 | (234) | 49 | (125) |
| $\delta_{s,max}$ | 111 | (282) | 55 | (140) |

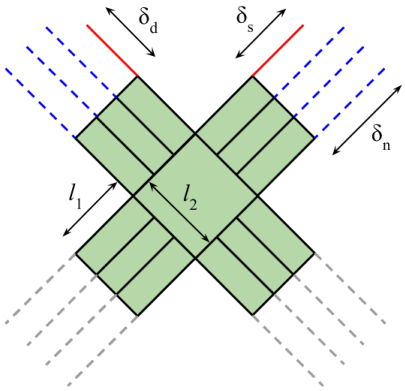


(b) Cruciform schematic.

Figure 4: Cruciform dimensions and schematic.

determined from an ellipsoid fit on collected data within the VST. Since the VST is composed mostly of steel, the magnetometer calibration was very sensitive to the position of the payload relative to the tunnel walls. Thus, calibration was performed often and it was necessary to verify that the measured heading calculated based on the compass calibration reflected the true physical heading of the parachute system in the tunnel. Verification was conducted qualitatively through successive $90^\circ$ rotations within the tunnel.

### 3.2.2 Test Setup

Along with the considerations with regard to the compass, additional changes were required to the vertical wind tunnel and the test article in order to facilitate the experimental program. To test the steerable cruciform in the NASA Vertical Spin Tunnel the parachute system was anchored in position inside the wind tunnel test section. Ideally the parachute system would free float inside the wind tunnel; however, for safety reasons, the parachute system was anchored in place thereby eliminating any potential for the canopy

to contact the fan.

The parachute system was equipped with a center anchor point located on the bottom of the payload enclosure near the center of gravity of the payload. This anchor was used to affix the parachute system to a system of rigging lines anchored to the bottom of the wind tunnel test section. A low friction swivel was used to attach the rotating canopy anchor line to the fixed wind tunnel anchor points. The swivel was included to allow the parachute system to rotate freely without storing energy as a torsional spring in the anchor line.

In order to facilitate easy removal and installation of the canopy into the test section between experiments, a light weight line was attached at the canopy apex. To speed up the experimental process the parachute system was simply allowed to land on the lower safety net between trials whenever possible. The parachute system was removed from the test section to change batteries by increasing the tunnel speed to float the system up, then guiding the parachute and payload through the test section opening using the upper guide line. Figure 5a shows the canopy as installed in the test section. The apex line is visible behind the canopy near the top of the image and the swivel anchoring is visible under the canopy safety net at the bottom of the image.

Since the steerable cruciform has a glide ratio on the order of $1 : 0.25$ to $1 : 0.50$, it was predicted that the parachute system would lean in the direction of glide during testing. Initial testing at the wind tunnel confirmed that that the canopy did maintain a pitch angle (typically $15^\circ$ to $35^\circ$). However, due to the limited height of the system as well as the tendency for large pitch angle to be naturally righted by the tunnel airflow, the

(a) Steerable cruciform system installed in the vertical spin tunnel.

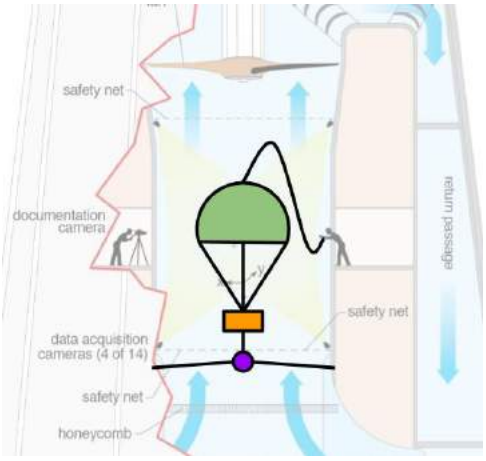


(b) Schematic of the test setup.

Figure 5: Experimental setup.

system was never at risk of contacting the walls of the test section.

### 3.2.3 Using Photogrammetry to Characterize Payload-Canopy Dynamics

To enable study of the relative motion between the payload and the canopy (relative) yawing, a camera (GoPro Hero3) looking up at the canopy was installed in the payload (the mount for this camera can be seen in Figure 2). The canopy featured two circular markers, one in the center of the canopy and another one at the base of the flap.

An image processing routine was developed based on finding the center of the cross canopy denoted by a red marker installed in the canopy. The radius of the marker as seen on the camera installed in the payload is only $5\,\mathrm{px}$ on average ($5\,\mathrm{px}$ is too small to be reliably detected by automatic identification; however, the developed algorithm is able to find the red marker in 91% of frames). Figure 6a shows an example of a successful

identification.

After finding the red center marker, each frame of the video is cropped relative to the center of the canopy (plus/minus $150\,\mathrm{px}$. At this point, the movement of a second (green) marker is detected. The movement of the second marker relative to the first marker defines the relative canopy-payload dynamics.

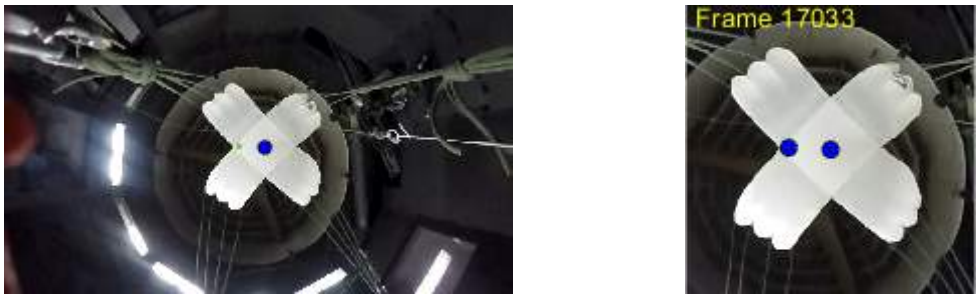


(a) Finding Canopy Center in Original Frame (red marker)

(b) Finding the Second (green) Marker

### 3.3 Aerodynamic Characterization

An interesting feature of the anchored test setup is the ability to approximately estimate the canopy glide ratio. However, the heading must be effectively stabilized in order to quantify the glide (this is true for both indoor and outdoor testing). The following section describes the efforts to develop a controller which can stabilize the yaw angle for the steerable cruciform system. Following development of the stabilizing controller, the closed-loop yaw model and glide ratio estimation methodology are described.

### 3.3.1 Heading Stabilization

The principal goal of the VST testing was to develop an effective proportional-integral-derivative (PID) controller to stabilize the canopy heading angle ($\Psi$). Physics suggests that the actuator command is indirectly related to the canopy heading rate ($\dot{\Psi}$). Specifically, the smaller the dynamic length ($\delta_d$), the faster the heading rate. However, the heading angle is the quantity of interest for the higher level navigation algorithm. In this study, the desired yaw angle is the reference input to the PID controller. A PID controller was chosen because of the simplicity in implementing this type of controller on the steerable cruciform hardware as well as the relatively slow physics of the vehicle.

$$\lambda = K_p e + K_i \int e, dt + K_d \dot{e} \tag{3.1}$$

$$e = \Psi_{\text{des}} - \Psi_{\text{meas}} \tag{3.2}$$

The performance of the controller was quantified with four metrics calculated from the output response to a step input with a magnitude of $90^\circ$. Step inputs were conducted for both positive and negative $90^\circ$ maneuvers. Recall that only a single actuator is dynamically actuated during a given experiment. Use of both positive and negative direction step responses enables estimation of the wind tunnel spin bias. A typical step response with important locations annotated is shown in Figure 7.

The first metric, rise time ($T_R$), was calculated as the duration after the initial application of the step input at which the output response first crossed the desired magnitude. Rise time is typically calculated as the time required to go from $10$ to $90\,\%$ of the

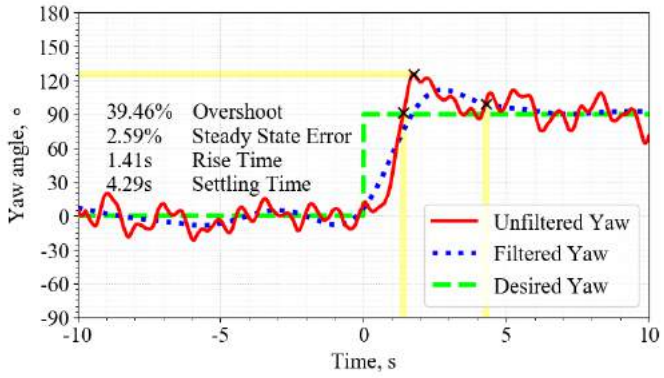


Figure 7: Typical step response, showing $OS$, $e_{ss}$, $T_R$, and $T_S$

final value. The persistent oscillations in the measured heading made this value difficult to identify for most of the experimental data. Thus, the modified rise time described here was used.

The second metric, settling time ($T_S$) was calculated as the duration after the initial application of the control signal at which a filtered estimate of the response variable achieved $90\,\%$ of the desired magnitude. Settling time is frequently calculated at $98\,\%$ of the desired magnitude; however, for the majority of trials this value was difficult to determine due to steady state oscillations in the response variable. Thus the requirement was relaxed to $90\,\%$ in order to allow more of the experimental data to be used in tabulating the controller performance.

The third metric, percent overshoot ($OS$), was calculated by comparing the magnitude of the extreme value of the response variable to the desired magnitude. Overshoot is expressed as a percentage even though the response variable and desired magnitude are both in degrees because it represents a ratio of these two quantities. The final metric, steady state error ($e_{ss}$) was computed by comparing the magnitude of the response

variable after settling to the desired magnitude. Steady state error is also expressed as a percentage.

### 3.3.2 Closed Loop Yaw Model Development and Characterization

Two systems were tested in the vertical wind tunnel. The larger of these systems makes use of the same payload, parachute, and rigging which was used for prior studies [17, 19]. Through this prior work it has been established that there is a persistent relative yaw oscillation between the payload and the canopy which occurs at approximately $1.0\,\mathrm{Hz}$. This relative motion is apparent in experiments where the system is observed to have a visually stable heading yet the measured heading shows a persistent and steady oscillation on the order of $10^\circ$ to $30^\circ$. Prior work to determine the functional form and coefficients for a model describing the open loop system behavior was confounded by these oscillations driven by relative motion.

Utilizing a canopy yaw model for controlled parachute simulations requires a model which relates an easily measured input variable to an easily measured output variable. Rather than estimate the bare airframe yaw dynamics, a closed loop model was identified which adequately reflects both the yaw dynamics and how the controller responds during descent. This closed-loop form captures the dynamics of the vehicle, the dynamics of the actuator, and the dynamics of the controller. The closed-loop model was easier to identify and of simpler form compared to models created for the open loop configuration. The steady state oscillations in the response variable (measured heading) are an impediment to developing a model which accurately captures the system dynamics.

These oscillations occur at a much higher frequency than the rest of the system dynamics and thus drive higher and higher model order in order to capture both the slow system dynamics and the high frequency oscillations. Thus it was necessary to filter both the input and output data prior to estimating model parameters.

The frequency of the relative motion is known to be approximately $1\,\mathrm{Hz}$, so this frequency was selected as a starting point for determining the appropriate cutoff frequency. Time domain analysis using different filter cutoff frequencies was conducted in order to determine exactly which behaviors in the time domain are associated with the slow, high power frequencies. A plot of measured yaw for a step input is included showing the results from three different cutoff frequencies in Figure 8.

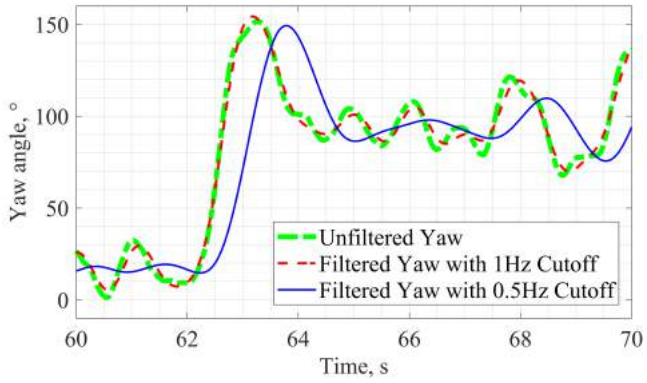


Figure 8: Measured yaw for different cutoff frequencies

From Figure 8 it can be seen that for a cutoff frequency of $0.5\,\mathrm{Hz}$ the yaw angle ($\Psi$) is smoothed but the dynamics which drive the large and slow change in response to the step input are still retained. The most obvious effect of such a slow cutoff frequency is to increase the rise time for the filtered response when compared to the measured response. For the purposes of this model, accurate rise time is less important than the low-frequency

motion.

Prior to performing closed-loop system identification analysis on the step response data, input and output variables for each experiment were filtered using a $4^{\text{th}}$ order, low-pass Butterworth filter with a cutoff frequency of $0.5\,\text{Hz}$. The system identification analysis was conducted using the MATLAB® System Identification Toolbox. Data was imported into the System Identification Toolbox grouped by experiments. There were between $2$ to $8$ trials for each experiment. Approximately 140 total trials were analyzed from the collected data. For this analysis, a trial is composed of data beginning just before and lasting for approximately $10\,\text{s}$ after the step input command was issued.

### 3.3.3 Glide Ratio Model Development and Characterization

Many airdrop systems rely on a non-zero glide ratio in order to achieve precision navigation and delivery. Controlling the heading of a system like the steerable cruciform only partially fulfills the requirements for developing a system capable of precision airdrop. In the case of the steerable cruciform, prior work [18] has characterized the glide performance of cruciform canopies according to different rigging configurations. For previously untested parachute systems there is often minimal prior information available on glide characteristics. The vertical wind tunnel testing provides a unique opportunity to quantify the approximate glide ratio capabilities of a canopy system through measurement of the pitch/roll angle of the system.

The dynamic equations which govern the behavior of the system must be modified from the free-flight condition to accommodate the anchoring constraints on the system.

The equations describing the constrained motion can then be manipulated using inverse kinematics to find an expression for glide ratio in terms of the ratio of the axial force ($F_A$) and side force ($F_S$) defined in the canopy body frame for a given tunnel speed. This relationship is shown in eq. (3.3).

$$GR = \frac{F_A}{F_S} \tag{3.3}$$

The schematic describing the simplified constrained system is shown in Figure 9. The instantaneous pitch angle is defined as the relative rotation about the body y-axis relative to the body-fixed yaw frame. The two dimensional simplification in the schematic is sufficient to characterize the motion because roll angle is not considered for this model.

During testing the canopy leans toward the test section wall according to the asymmetrical rigging for glide. The joint at A is modeled as a revolute joint (simplified from a spherical joint in three-dimensions). The link between A and P, which was actually a cord, is considered to be a rigid link and the connection between the payload and rigid link AP is considered to be rigid connection. These simplification are made out of necessity as no additional data is available which gives the relative angle between the taut suspension cord and the payload. Higher accuracy in the glide ratio estimation could be obtained by measuring the angle of this link; however, in the absence of this extra information, the modeling assumptions explained above allow a reasonable approximation of glide ratio to be found.

A symbolic dynamics software package (Motiongenesis) was used to generate the equations of motion for the constrained system for the axial and side force and are given

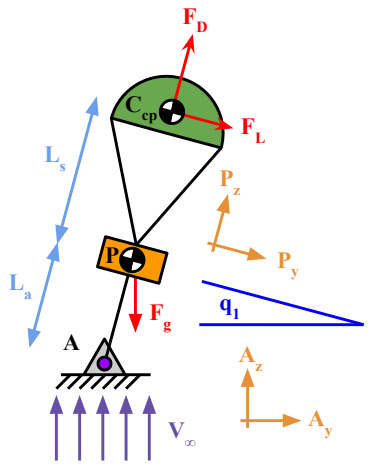


Figure 9: Schematic for dynamic model of constrained parachute system

in Eqs. (3.4) and (3.5).

$$F_A = \frac{-0.0833 m_p \left[(12)\sin(q_1)(g - L_a u_1^2 - \dot{u2}) - (b^2 + h^2 + 12L_a^2)\cos(q_1)\dot{u}_1\right]}{L_a + L_s} \tag{3.4}$$

$$F_S = \frac{0.0833 m_p \left[(12)\cos(q_1)(g - L_a u_1^2 - \dot{u2}) - (b^2 + h^2 + 12L_a^2)\sin(q_1)\dot{u}_1\right]}{L_a + L_s} \tag{3.5}$$

The symbolic equations of motion produced are algebraically solved for the axial force and side force ($F_A$ and $F_S$ respectively). These equations are coded in MATLAB®. The MATLAB® script accepts the time history of the pitch angle relative to the earth frame (and its derivatives) and outputs instantaneous GR versus time. The pitch angle relative to the earth frame was recorded for all experiments at $100\,\mathrm{Hz}$. The pitch rate and pitch acceleration were found by taking first and second numerical derivatives of the pitch angle. The resulting estimates for pitch rate and pitch acceleration were corrupted by large magnitude high frequency noise, thus a $12^{\text{th}}$ order Butterworth, low-pass filter with a cutoff frequency of $1.0\,\mathrm{Hz}$ was applied to all sensor and actuator values.

## 3.4 Results and Discussion

This section discusses the results of VST testing of cruciform parachute systems. First, some qualitative results are presented, followed by results for the stabilization controller. Then the results for the closed-loop yaw model are presented and the section ends with a discussion of the GR estimation results.

### 3.4.1 Effect of Suspension Line Deflection on Heading Rate

Since the parachute system was modified slightly to accommodate the requirements of the vertical wind tunnel, it was necessary to investigate the effects these modifications might have on the system behavior. Knowledge of the type and quantity of the effects of these modifications is required in order to evaluate the validity of the results obtained during wind tunnel testing.

To prevent the canopy from colliding with the sides of the tunnel, the canopy was secured in the center of the tunnel. Excessive glide could induce a change in pitch angle (forward lean) which could lead to the canopy contacting the walls. Prior work by Potvin demonstrated that the glide tendency could be modified by altering the length of the control lines [18]. However, no data had previously been collected which investigated what effect increasing or decreasing glide trim had on the heading rate dynamics of the system. To study the effect of suspension line length on the heading dynamics, the length of the dynamic line was commanded to sweep slowly from the minimum length (shorter than the static line length) to the maximum (longer than the static line length). The static line deflection was changed to a different fixed value prior to each experiment. Data from

these experiments was used to characterize the general shape of the system response curve in terms of varying static line deflection as well as to study the maximum possible heading change rate for a given set of conditions.

Results showing the relationship between heading rate and static line length are presented in Figure 10. Each line represents a different experiment with a unique value for the static suspension line length. In general, it was found that the heading rate is not strongly related to the static line length. In fact, the heading rate has a nearly linear relationship with normalized deflection of the dynamic line up until the point of saturation or canopy collapse. By extension, if the heading rate is not significantly affected by changing the suspension line deflection, then the heading rate characteristics are not dependent on the glide ratio. Knowledge that heading rate characteristics were mostly unaffected by the length of the static line allowed further experiments to go forward with the assurance that trimming the system for minimum glide to decrease the likelihood of the canopy contacting the tunnel walls would not lead to results which varied significantly from the dynamics expected when the canopy is rigged for maximum glide.

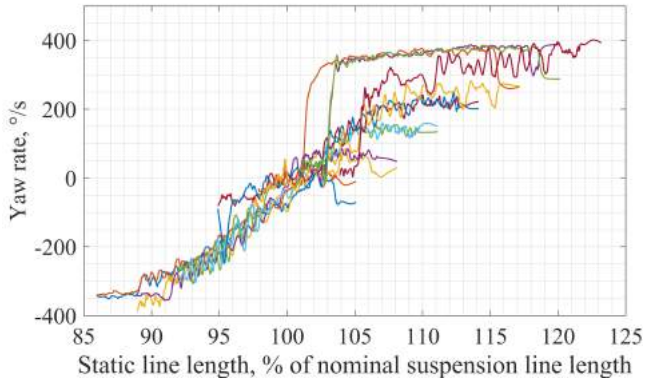


Figure 10: Heading rate vs. amount of dynamic line deflection

### 3.4.2 Relative Canopy Motion

Figure Figure 11a shows an example of one video file processed. This file has 17033 frames in it, recorded with a 239.7622 frame rate, i.e. represents 71-second test sequence. Figure 11b provides the very first 10 seconds of this sequence. The upper portion of Figures 11a and 11b show time history of the computed distance between two markers (in pixels). This distance was used to eliminate computed data outliers. Lower portions of Figures 11a and 11b represent time histories of the canopy yaw angle with respect to the payload box.

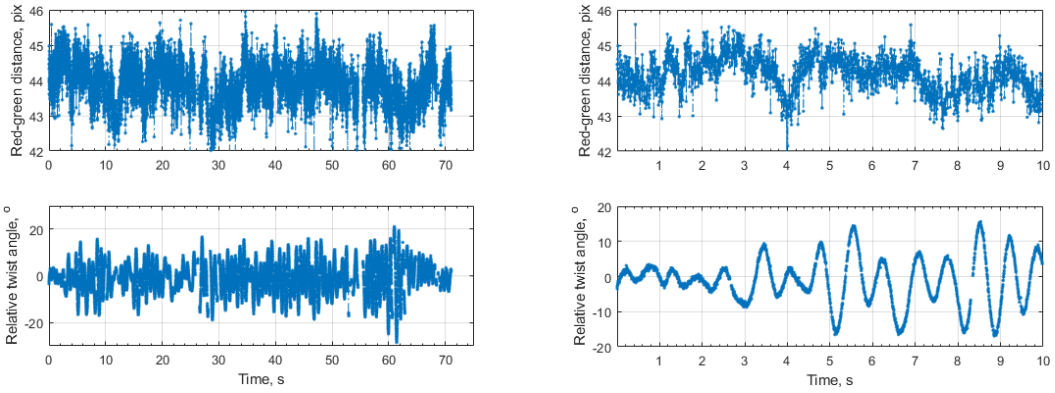


(a) Time history of computed distance between markers (full trial, over 60s)

(b) Time history of computed distance between markers (10s)

In this test, the parachute system was stabilized first to eliminate a constant rotation (by the payload box). In this stabilized condition, the canopy oscillates around a nominal (zero value) with a magnitude of about $5^\circ$ at about $1.5\,\mathrm{Hz}$ (Figure 12). When the control commands are applied (the parachute system is put in a spin), the canopy oscillation magnitude increases to about $15^\circ$. This result correlates well with the previously estimated relative motion results indicated approximately $1.0\,\mathrm{Hz}$ oscillations.

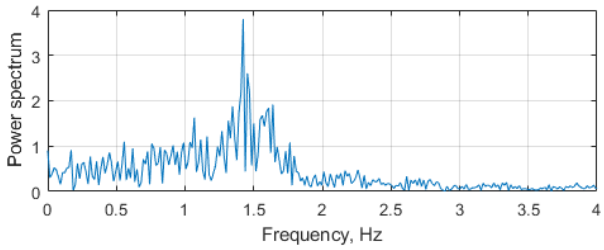


Figure 12: Relative yaw angle power spectrum

### 3.4.3 Heading Stabilization Controller

To reiterate, the primary goal of the experiments conducted at the vertical wind tunnel was to develop a heading stabilization controller. To that end, a controller was developed which sufficiently stabilized the system heading in the wind tunnel under a variety of conditions. Different tunnel speeds, different payload weights and two different canopies with different geometry were used during the week long testing event. The controller developed at the vertical wind tunnel was also tested under outdoor flight test conditions for verification. During the outdoor flight testing, the system was observed to be overexcited and the controller gains were reduced. The corresponding gains were reduced by approximately $50\%$. The resulting performance was more favorable and analysis of the flight data showed similar step input response to the vertical wind tunnel data. Though the controller needed to be scaled, the proportionality between the gains did not need to be changed. This supports the conclusion that the controller developed using vertical wind tunnel methodology is applicable under flight conditions in the context of reducing outdoor testing efforts needed to create suitable steering control systems.

The heading stabilization controller was characterized by analyzing the $190$ individual experimental data sets. The average results grouped according to which canopy

was used are shown in Table 1. The small canopy was prioritized over the large canopy due to the lack of control improvement for the large canopy observed in the vertical wind tunnel. Therefore, there is no outdoor flight test data available for the large canopy. However, results from experiments conducted with the small canopy during outdoor flight testing is shown. As a reminder the control gains were reduced by $50\%$ to reduce the overexcited control in outdoor testing (with identical scaling to the VST-determined gains).

Table 1: Performance of stabilization controller

| | **Big canopy** | **Small canopy** | | |
|---|---|---|---|---|
| | Spin Tunnel | Spin Tunnel | Flight Test | |
| *Parameter* | *Value* | *Value* | *Value* | *Difference* |
| $OS$ | $52\,\%$ | $71\,\%$ | $34\,\%$ | $52\,\%$ |
| $e_{ss}$ | $3.1\,\%$ | $2.1\,\%$ | $2.4\,\%$ | $17\,\%$ |
| $T_R$ | $1.2\,\mathrm{s}$ | $1.2\,\mathrm{s}$ | $2.4\,\mathrm{s}$ | $100\,\%$ |
| $T_S$ | $5.6\,\mathrm{s}$ | $6.5\,\mathrm{s}$ | $5.8\,\mathrm{s}$ | $11\,\%$ |

It is expected that the percent overshoot will be smaller and $T_R$ will be larger for flight testing since the gains were reduced to alleviate over excitation and consequently the transient response is expected to be slowed. The relatively small values for steady state error support the conclusion that the steerable cruciform system is capable of precision navigation. Additionally, the close match between the flight test results and the spin tunnel results further support the conclusion that the spin tunnel experimental methodology closely mimics the dynamics of outdoor flight testing.

Even though the gains needed to be scaled, the proportion between the three gains remained the same. Previously, the number experiments needed to successfully tune the controller gains was an obstacle to the development of a suitable controller. Even if the

a controller developed at the VST is not perfectly suited for flight testing, the ability to tune the system simply by scaling the magnitude of the three gains while keeping the proportion the same reduces the complexity and time associated with tuning the system for free-flight conditions.

### 3.4.4 Closed Loop Yaw Model

Data used to identify the closed loop yaw model was first filtered according to a $4^{\text{th}}$ order, low-pass, Butterworth filter with a cutoff frequency of $0.5\,\text{Hz}$. Filtering at such a slow frequency is acceptable because the higher frequency information is not critical to characterize the motion of interest. It is important to understand that even if the high frequency oscillations collected by the instrumentation located in the payload represented physical motion and not just noise, that the effect on the motion of the canopy with its large effective inertia would be very small. The oscillations measured at the payload are not necessarily reflective of the overall motion of the canopy and therefore not critical to a simulation intended to capture the long-term dynamics needed for a navigation simulation. The relative motion may potentially affect the simulation but without additional information on the heading of the canopy itself, there is not way to quantify this effect and so it is ignored for now.

The second order transfer function model structure was selected because it provided the closest match to the experimental data without over fitting. Consequently, the second order transfer function model matches nicely with a basic intuitive understanding of the system physics. For a stable closed-loop system, it is expected that the input

and output are separated by a time delay and some ripple in the magnitude. The general equation for the second order transfer function is given in Eq. (3.6).

$$H(s) = \frac{As + B}{s^2 + Cs + D} \tag{3.6}$$

Several other model structures, including higher order transfer functions and polynomial models were investigated. Over fitting was quantified by using the model created from one data set to predict the output response from a verification data set and then comparing the predicted and measured outputs. The best model structure was selected by comparing the training and test error for various scenarios. The simple second order transfer function structure represents the highest order model which was not prone to over-fitting the data. Average coefficients were estimated for one set of PID gains which stabilized both the large and small canopy. The average coefficients for both canopies combined are presented in Table 2.

Table 2: Overall average coefficients for 2nd order transfer function model

| **Coefficient** | **Value** |
|---|---|
| A | 0.72 |
| B | 2.1 |
| C | 1.3 |
| D | 2.1 |

The output response for a step input with magnitude equal to $90^\circ$ for a transfer function created with the previously identified coefficients is shown in Figure 13. Also plotted are the raw and filtered measured headings from a typical step input trial.

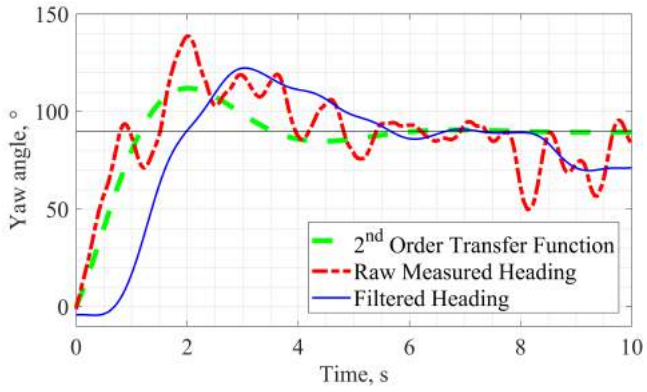


Figure 13: Step input response for 2nd order transfer function model

The resulting transfer function model was subjected to a step input so that the output response from the identified transfer function could be compared to the four metrics used to characterize the controller on the physical system ($T_R$, $T_S$, $OS$, and $e_{ss}$). The characteristics of the transfer function model found from the output response for more than 100 trials are listed in Table 3.

Table 3: Output response to step input for 2nd order transfer function model

| **Parameter** | **Value** | |
|---|---|---|
| $OS$ | 26 | % |
| $e_{ss}$ | 4.7 | % |
| $T_R$ | 0.90 | s |
| $T_S$ | 1.3 | s |

From the step response characteristics shown in Table 3 as well as from looking at the curves shown in Figure 13 it can be seen that percent overshoot of $26\,\%$ for the identified transfer function is smaller than the percent overshoot measured during spin tunnel experiments and smaller than the percent overshoot measured during flight tests. The value for $e_{ss}$ of less than $5\,\%$ from the transfer function is of approximately the same

magnitude as the small $e_{ss}$ seen for all the experiments on the physical system. The values for $T_R$ and $T_S$ according to the transfer function model are smaller (faster transient response) than the values measured during the wind tunnel and flight test experiments. Values for $T_S$ and $e_{ss}$ should be smaller since the transfer function model is based on a filtered version of the measured heading. Importantly, the step response for the transfer function model closely matches the initial transient response of the unfiltered measured heading.

### 3.4.5 Glide Ratio Model

In addition to developing a heading controller and identifying the closed-loop dynamics, the vertical spin tunnel data was extended to approximate the GR as a function of pitch angle. Determination of glide ratio is very important in terms of precision guidance capabilities, thus any method which enables glide ratio estimation from experiments conducted in the controlled VST environment in an efficient manner provides a cost efficient yet data rich test program.

Instantaneous, simulated glide ratio data was filtered according to a $12^{\text{th}}$ order Butterworth, low-pass filter with a cutoff frequency of $1.0\,\text{Hz}$. In this case, the low cutoff frequency is justified in the sense that the purpose of the glide ratio model is to capture the long-period gliding motion of the canopy and not the fast fluctuations associated with disturbances such as those due to the wind. Even if high frequency variations in the time signal are due to the actual motion of the system, removing this motion from the signal by filtering will have a small effect on the overall glide ratio estimate. A plot of glide ratio

versus time for a typical experimental trial is shown in Figure 14.

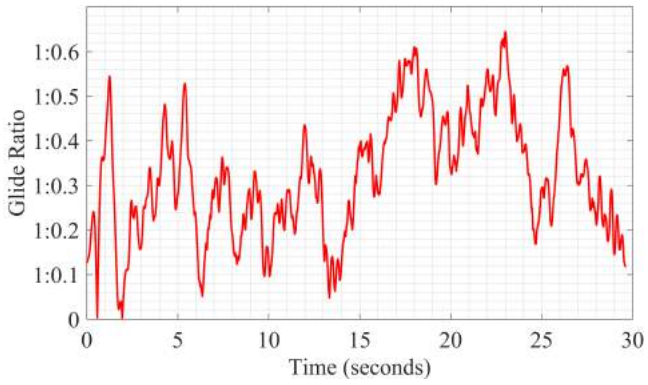


Figure 14: Typical instantaneous glide ratio for VST data

Glide ratio for the steerable cruciform has been experimentally determined previously to be $1 : 0.25$ to $1 : 0.50$ [17]. This is consistent with glide ratio estimates for similar canopies evaluated by Potvin et. al. [18]. As discussed by Fields and Yakimenko, the glide ratio estimate from outdoor flight testing is conservative because it does not account for inefficiencies associated with imperfect heading control including along an oscillatory path [17].

Data from 90 experimental trials from the vertical wind tunnel was collected and average glide ratio was computed. The resulting overall glide ratio for the spin tunnel experiments was found to be $0.3065$. The glide ratio from the fixed heading outdoor flight tests was found to be $1 : 0.2850$. Thus, the simulation results in an estimate of glide ratio which is close to the GR seen during flight testing. In fact, the simulated GR is about $7\,\%$ larger than the measured glide ratio from outdoor flight testing.

The ultimate goal of this work is to lay the groundwork for a methodology which can be used to vet new untested parachute systems in a highly cost effective manner. If

spin (heading) and translational (glide) characteristics can be studied during a constrained experiment inside of a vertical wind tunnel then all the experimental testing needed to characterize, control and simulate a previously unknown system can be conducted in a highly efficient manner. The steerable cruciform is sufficiently small such that a full-scale model was able to be tested in the wind tunnel. The methodology presented here is applicable to small parachute systems with light payloads as well as scale models representing larger systems.

## 3.5 Vertical Wind Tunnel Experiment Conclusions

The steerable cruciform parachute system bridges the gap between parafoil systems and low-accuracy unguided airdrop systems. The simple concept relies on only a single actuator in order to accomplish precision navigation using a low-cost canopy. Precision navigation is possible because the heading of the canopy can be controlled via asymmetrical deflection of control lines while glide can be induced via symmetrical deflection.

In order to demonstrate the precision navigational abilities of the system, a heading stabilizing controller was needed. Attempts to design this controller during outdoor flight testing proved unfruitful due to a number of factors including limited time of descent. Vertical spin tunnel testing was selected as an experimental method which would allow a controller to be developed in a more controlled environment compared with outdoor flight tests.

Experiments were conducted in the NASA 20 ft. Vertical Spin Tunnel with the

parachute system tethered in place. A heading stabilizing controller was developed first as the primary motivation behind the experiment and also the most fundamental requirement for precision navigation. Once the heading could be stabilized by the control system, other experiments were conducted to enhance the usefulness of the experimental program.

A model describing the closed-loop system relating the system heading to the commanded heading was identified from VST data. This model is useful for simulating the performance of the system in response to different navigation algorithms. A technique was developed for determining glide ratio based on a simplified dynamic model of the system as installed in the wind tunnel. Despite the simplifying assumptions, the estimated glide ratio corresponds with outdoor glide ratio estimates.

Building on prior work, the relative yaw motion between the payload which contains the attitude sensors and the canopy was studied using photogrammetry. This analysis supports prior conclusions about the relative yaw motion between the payload and the canopy. Specifically, there is a persistent oscillation at approximately $1.0$ to $1.5\,\mathrm{Hz}$ with a magnitude of approximately $5$ to $15^{\circ}$.

The experiments conducted at the VST have dual benefits. Firstly, a control system for the steerable cruciform parachute system was able to be developed quickly. The resulting control system was adapted for flight testing with minimal effort. Additionally, closed-loop dynamics and glide ratio were able to be estimated based on experimental data. Secondly, the VST methodology itself was proven to a be a viable method for rapid testing and development of new parachute control techniques. This methodology could be used to conduct preliminary screening experiments on new canopy shapes or rigging

configurations without substantial outlay of resources.

# CHAPTER 4

# INVESTIGATION OF NAVIGATION STRATEGIES

This chapter details an investigation into strategies which allow the SnowflakeX system to navigate autonomously in the earth frame. Through both simulation and outdoor flight testing, various strategies are investigated and characterized according to how closely the landing point corresponds to the desired impact point. Four different flight tests are described and the results are presented. A simulation is developed which is verified against data collected from outdoor flight tests. Following verification, the simulation is used to generate many simulated drops which are used to characterize the system performance under varying levels of wind uncertainty. Conclusions based on the findings are then presented along with potential future directions for the SnowflakeX system development.

## 4.1 Methodology

### 4.1.1 Explanation of Reference Frames and Common Terms

Miss distance as well as miss direction will be used throughout this work to describe the difference between the desired impact point on the ground and the landing location for both simulated and measured cases. The miss distance will be reported in feet ($\mathrm{ft}$) and the miss direction will be given in degrees ($^\circ$). Figure 15 demonstrates graphically how the miss distance and miss direction are calculated for an example drop.

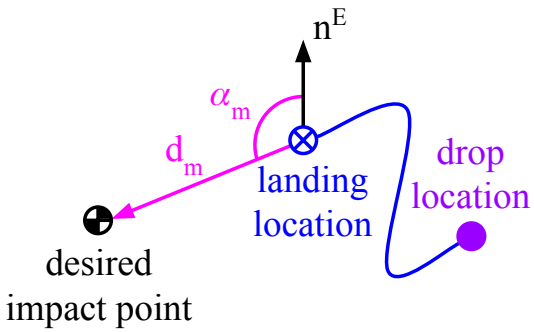


Figure 15: Graphical illustration of miss distance and miss direction for a sample drop

The coordinate system used is the north-east-down coordinate system. In the earth fixed frame, the positive north axis always points in the direction of true north, the positive east axis always points in the east direction and the positive down axis points down toward the center of the earth. In the payload fixed frame the positive north axis always points forward in the direction of glide, the east axis always points out the right side of the payload and the down axis points downward along a vector which goes from the center of the canopy through the center of the payload. For the simulation, the dynamics are reduced such that pitch and roll motion are ignored and thus the payload fixed frame is related to the earth fixed frame by a planar transformation based on the yaw angle. Both coordinate frames as well as the relationship between the yaw angle ($\Psi$) and the orientation of the payload fixed frame in the earth fixed frame is shown in Figure 16.

Circular error probable (CEP) is used throughout this work to characterize the central tendency of miss distance. CEP is defined in this context in the following way. First, each measured landing location is compared to the desired impact point for that particular drop. The miss distance and direction are recorded. The CEP is found as the

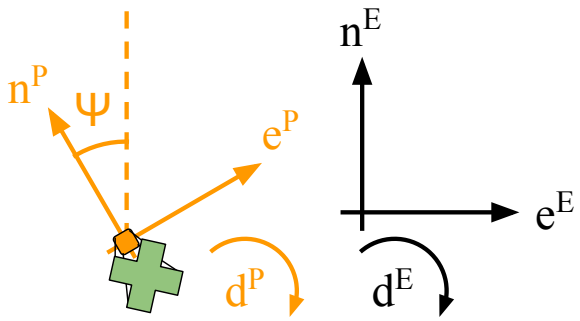


Figure 16: Illustration of coordinate frames and relationship with payload yaw ($\Psi$)

median value of all the recorded values for miss distance. This convention generates a CEP that is primarily a measure of precision in the landing location data.

During the simulated experiments, it is necessary to speak in terms of two distinct wind measurements. These wind measurements are defined here for clarity. The wind measurement used to generate the ballistic trajectory will be referred to as the waypoint winds or the original wind measurement. In contrast, the wind measurement which is to be used to simulate the real winds in the dropzone will be known as the dropzone winds or the simulation wind measurement.

Additionally, when talking about the distinct wind measurements, quantities will be introduced to characterize the two wind measurements and the difference between them. The prevailing wind direction and distance are given by the distance and heading from the first waypoint in the ballistic trajectory to the last waypoint in the ballistic trajectory. The difference between the distances for two wind measurements and the difference in the direction between the two wind measurements will also be used as quantities of interest. This process is shown graphically in Figure 17

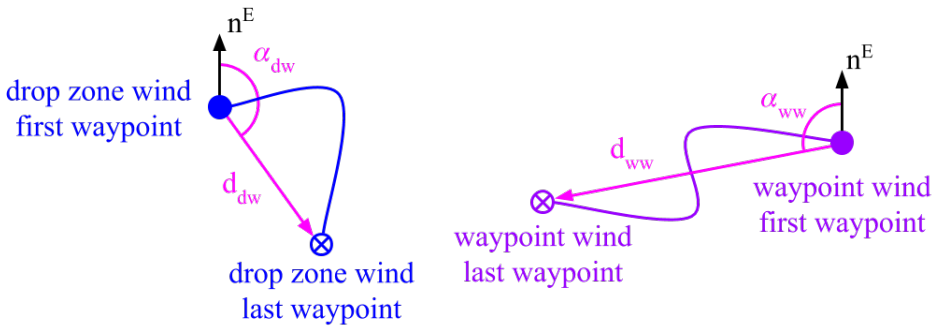


Figure 17: Illustration of wind characterization for waypoint and drop zone wind measurements

During the verification of the simulation, instead of miss distance and miss direction, the residual in the miss distance and miss direction is used. The residuals are found by subtracting the simulated miss distance and miss direction from the measured miss distance and miss direction respectively. In the case of residuals, CEP will not be used in order to avoid confusion. Instead average residual miss distance will be reported.

### 4.1.2 Flight Test Procedures

This paper presents results from four separate outdoor flight test events conducted over three locations over the last 12 months. Two of these events involved drops from manned aircraft and the other two events were conducted using UAV flown by UMKC researchers. The following procedure applies specifically to the UAV test events. However, while the logistics of dropping from manned aircraft are very different, the general shape of the procedures is similar. For example, wind information is obtained the same way for drops conducted from UAV as well as manned aircraft. Additionally, in order to smooth the transition from unmanned to manned drop aircraft, the UAV drop procedures

have been designed to mimic the manned aircraft drop procedures as closely as possible.

For unmanned flight testing a large UAV is outfitted with a radio-controlled (RC) drop system. The UAV is a $1400\,\mathrm{mm}$ class and has payload capacity of approximately $40\,\mathrm{lbf}$. The UAV is limited to a maximum altitude of approximately $5000\,\mathrm{ft}$ above ground level (AGL) by the limited range of the ground telemetry system. Drop testing was conducted at Camp Roberts, CA in restricted airspace.

For each sortie, the UAV payload comprises one SnowflakeX aerial guidance unit (AGU) with parachute in addition to a simple dropsonde AGU with a separate parachute. The dropsonde parachute is a simple flat circular parachute reefed to match the SnowflakeX descent rate as closely as possible. The dropsonde AGU contains a GPS logging device which records GPS position in 3-dimensions ($r_x^E$, $r_y^E$, $r_z^E$) at $1\,\mathrm{Hz}$.

After flying the UAV up to the drop altitude, the UAV is piloted to the CARP and commanded to hold the current GPS position. Most of the drops conducted made use of persistent point toward target navigation with a pilot determined approximate CARP. For these drops, the pilot uses knowledge of prior winds as well as an estimate of the winds during ascent to determine the best drop location.

Once the UAV is in the correct position, the wind parachute is released from he UAV by RC transmitter. All drops are conducted with the UAV in a fixed position relative to the earth frame, the velocity of the UAV in the inertial reference is 0 in all three dimensions ($v_x^E = v_y^E = v_z^E = 0$). Following a short pause to allow separation between the two payloads, the SnowflakeX parachute and payload system is released via RC transmitter.

The guided SnowflakeX parachute and payload steers toward the target and the

dropsonde falls according to the wind. Once the dropsonde is recovered, the GPS ground track is downloaded and a smooth continuous ground track is created using a cubic spline interpolation. The dropsonde instrumentation only updates the GPS information at $1\,\mathrm{Hz}$ and the interpolated track allows the data to be used in application requiring more granularity. The smooth GPS track includes a continuous altitude vector which can be used to scale the effect of the wind to match a system with a different descent rate. In this case, the average descent rate of the SnowflakeX system is $22\,\mathrm{ft/s}$ whereas the dropsonde descent rate, though matched to the SnowflakeX system by reefing, varies somewhat from drop-to-drop. A ratio of the measured GPS descent rate and the average measured SnowflakeX descent rate is used to stretch the GPS ground track to account for a slower descending parachute and payload system or shrink the GPS ground track to account for a faster descending parachute and payload system.

To develop the reference waypoint trajectory, the interpolated ground track is sampled starting from the ground up at uniform altitude intervals. The altitude dependent waypoint track is shifted so that the end waypoint is coincident with the desired impact point on the ground. If the SnowflakeX system is using the waypoint navigation technique then the resulting waypoints are uploaded to the AGU. In any case, the topmost waypoint is taken as the CARP and used as a reference to help the pilot position the UAV. The interpolated GPS ground track is recorded along with the date and time and the maximum altitude for the drop.

### 4.1.3 Modeling Simplifications

A numerical simulation was developed in order to allow navigation strategies to be studied in a control environment prior to flight testing. The simulation makes use of reduced payload-parachute system dynamics in order to propagate a trajectory in three dimensional space based on the wind conditions in the simulated drop zone. For the simulation, the parachute system is treated as a particle located at the center of mass of the payload. The effective inertia of the canopy is ignored and the velocity in the payload frame is constrained to occur in the forward direction only (no side-slip). The dynamics are further reduced by assuming the payload velocity in the downward direction is constant ($22\,\mathrm{ft/s}$). The rolling and pitching motion of the payload system are ignored and thus the velocities in the body fixed frame are related to the velocities in the earth fixed frame by a rotation matrix based on the yaw (which is defined in the fixed earth frame). The reduced state equations describing the velocities in the payload frame are given in Eq. (4.1).

$$\underline{v}^P = \begin{cases} v_n^P & = GRv_d^P \\ v_e^P & = 0 \\ v_d^P & = 22\,\mathrm{ft/s} \end{cases} \tag{4.1}$$

The simulation in the payload frame is then reduced to simple kinematic relationship for the case of constant velocities. The equations describing the three-dimensional

motion in the payload fixed frame are given in Eq. (4.2).

$$\underline{v}^P = \begin{cases} r_n^P & = r_{n0}^P + v_n^p dt \\ r_e^P & = r_{e0}^P = 0 \\ r_d^P & = r_{d0}^P + v_d^P dt \end{cases} \tag{4.2}$$

Since the simulation is numerical, the equations of motion must be transformed to the discrete form. For the discrete form, the index $k$ refers to the current iteration while $k+1$ and $k-1$ refer to the next step and the previous step respectively. Using this convention, the equations in Eq. (4.2) and transformed into the form shown in Eq. (4.3).

$$\underline{v}^P = \begin{cases} r_n^P(k) & = r_n^P(k-1) + v_n^p dt \\ r_e^P(k) & = r_e^P(k-1) = 0 \\ r_d^P(k) & = r_d^P(k-1) + v_d^P dt \end{cases} \tag{4.3}$$

The recorded wind effects are defined in terms of the inertial earth fixed frame. Additionally, the navigation tasks are defined in the inertial fixed frame. Thus, it is necessary to transform the payload position into the inertial earth fixed frame by the rotation matrix given in Eq. (4.4). The common shorthand is used whereby $c_\Psi$ refers to $\cos(\Psi)$ and $s_\Psi$ refers to $\sin(\Psi)$.

$${}_E R_P = \begin{bmatrix} c_\Psi & s_\Psi & 0 \\ -s_\Psi & c_\Psi & 0 \\ 0 & 0 & 1 \end{bmatrix} \tag{4.4}$$

The numerical simulation was developed using nine working navigation drops from prior flight testing as a training dataset. Most of the simulation is based on simplified kinematic relationship with velocities in the payload frame set to zero. The dynamics

relating the input desired heading ($\Psi_d$) to the measured heading of the payload ($\Psi$) was identified based on data collected in a vertical wind tunnel experiment. The relationship was formulated in transfer function form and is given in Eq. (4.5).

$$\frac{\Psi_d}{\Psi} = \frac{0.72s + 2.08}{s^2 + 1.27s + 2.09} \tag{4.5}$$

To use this continuous transfer function in a numerical simulation, the discretized transfer function must be used. The discretized transfer function is given in Eq. (4.6).

$$\frac{\Psi_d}{\Psi} = \frac{0.0073z + 0.0071}{z^2 + 1.99z + 0.99} \tag{4.6}$$

It is convenient to put the transfer function in digital signal processing form. The resulting expression is given in Eq. (4.7).

$$\Psi(1 - 1.9z^{-1} + .99z^{-2}) = \Psi_d(0.0073 - .0071z^{-1}) \tag{4.7}$$

Putting the equation in eq. (4.7) into the previously used discrete form using index $k$ and solving for the desired quantity measured yaw ($\Psi$) yields eq. (4.8).

$$\Psi(k) = 0.0073\Psi_d(k-1) - 0.0071\Psi_d(k-2) + 1.9\Psi(k-1) - .99\Psi(k-2) \tag{4.8}$$

The simulation is performed in a number of steps. The ordering of these steps is designed to mimic the order of sensor sampling and computation which occur on the AGU in real-time during outdoor flight testing. The steps and their order is given in Table 4.

Table 4: Simulation steps

| Step | Description | Physical Analog |
|---|---|---|
| 1 | Find the current value of desired yaw ($\Psi_d(k)$) | Desired yaw is calculated at the beginning of the control loop using the current gps position and waypoints |
| 2 | Find the current value of yaw ($\Psi(k)$) using the transfer function | The measured yaw at the current time step is available prior to each iteration of the control loop |
| 3 | Update the payload position in the fixed earth frame ($\underline{r^E}$) according to the forward velocity at the current time step | The canopy is always translating in the direction of the measured heading |
| 4 | Update the payload position in the fixed earth frame ($\underline{r^E}$) according to the direction and velocity of the wind at the current time step | The effect of the wind is unknown to the system in real time, thus the wind should be added last prior to updating the measured variables for the next simulation step |

Important simulation constants are given in Table 5. During the development and evaluation of the simulation, it was necessary to introduce the tuning parameter *GR Reduction* to account for the glide which is lost during outdoor flight tests due to the high frequency oscillations in heading. These oscillations are not present in the simulation because the heading transfer function was identified using filtered data.

To determine the appropriate value for *GR Reduction* a screening experiment was conducted where the distance and direction between the measured payload landing location and the simulated landing location were compared for each available drop. The *GR Reduction* was allowed to vary between $50\,\%$ to $100\,\%$ in steps of $10\,\%$.

Table 5: Simulation parameters

| **Parameters** | **Value** | **Descriptive Name** |
|---|---|---|
| GR | 0.35 | Glide ratio |
| GR Reduction | $87.5\,\%$ | Tuning parameter |
| $v_d^E$ | $22\,\mathrm{ft/sec}$ | Descent rate |
| $dt$ | $0.01\,\mathrm{sec}$ | Time step |
| Altitude Step | $100\,\mathrm{ft}$ | Waypoint altitude spacing |

Successive screening experiments were conducted and the range of *GR Reduction* was reduced and the granularity of the search was increased at each step. Ultimately a *GR Reduction* of $87.5\,\%$ was selected. The miss distance and direction between each simulated drop and the corresponding measured drop was recorded for each value of *GR Reduction*. In the final screening experiment, the residual distance for all values of *GR Reduction* became mostly uniform. The final decision for value of *GR Reduction* was based on the most uniform residual direction in addition to the residual distance. The distribution of the misses as measured by the residual direction for a *GR Reduction* of

87.5 % resulted in a low value for average residual distance between the simulated and measured cases as well as showing a visually uniform distribution of misses in terms of residual direction.

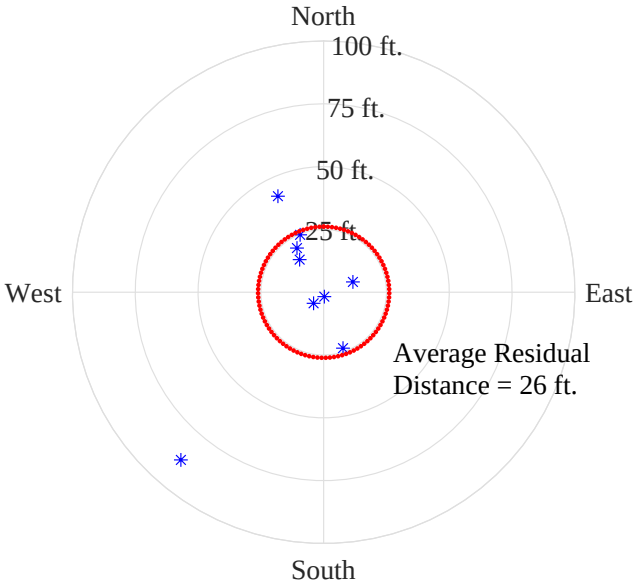


Figure 18: Simulation verification using GR reduction of 87.5 %

### 4.1.4 Simulation Verification

Results of the simulation validation are presented in Figure 18. For this plot, the distance and direction of the simulated landing location is found as the miss distance and direction based on the nominal measured trajectory. Results for all the drops are plotted with the center point representing the case where the simulated and measured landing locations coincided perfectly. The CEP on the plot shows that half of the simulations resulted in a difference of less than 21 ft compared to the measured landing location.

### 4.1.5 Simulation Structure

The simulation was also used to evaluate the performance of different navigation schemes in response to uncertain winds. Uncertainty in the CARP was also introduced. Prior to performing a simulation each measured wind file was characterized according to two metrics. The overall wind direction was found by computing the angle between the starting and ending coordinates for the ballistic waypoints. The overall wind distance was found by computing the distance between the starting and ending coordingate for the ballistic waypoints.

The ideal CARP is still taken as the starting coordinates for the ballistic trajectory. However, other drops are simulated based on erroneous CARP locations. Using the overall wind direction to define a local wind fixed coordinate system, one simulated drop is started at each of the four cardinal directions at a radius equal to $5\,\%$ of the drop altitude away from the ideal CARP. According to this method there are a total of five drops for each simulated trial. One drop occurs perfectly at the CARP, another drop occurs in the same direction as the overall wind direction, another in the opposite direction from the overall wind direction. Then two drops occur perpendicular to the overall wind direction, one each way.

One bundle of drops is conducted for each navigation scheme for each trial. In this way there are a total of five drops for each of two navigations schemes for each simulated trial. Thus there are a total of ten drops available for each set of simulation conditions. The total number of available simulation conditions is given by all possible combinations of input wind files according to the following rules. One set of wind files is

used to generate the ballistic trajectory and thus the waypoints. A unique set of wind files is used to represent the simulated winds in the drop zone. The wind files representing the wind in the drop zone must include all possible altitudes available in the wind files used to generate the waypoints. Thus the number of combinations of wind files is limited to include only those simulations were the altitude of the second wind file is greater than the altitude of the original file. From 37 possible wind files, more than 450 unique simulated combinations are available.

Additionally, for most trials, the actual drop point was varied from the CARP by an amount equal to $5\,\%$ of the maximum altitude in the original file in each of four direction. The prevailing wind direction was computed as the heading angle between the CARP and the desired impact point. One drop point was placed in the direction of the prevailing wind and another was placed opposite the direction of the prevailing wind (farther from the target). Similarly, the other two drop points were placed perpendicular to the prevailing wind direction, one in each direction. Figure 19 shows graphically how the drops in each simulation trial are distributed.

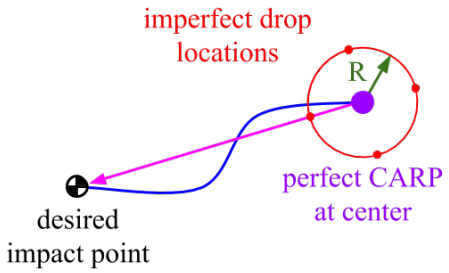


Figure 19: Illustration of drop locations for simulation trials

### 4.1.6 Logistic Regression Classifier

A simpler technique to improve the impact point accuracy of the SnowflakeX system was investigated. A substantial difference was observed in the performance of the two navigation schemes depending on whether the winds in the dropzone were known with or without error.

In order to determine which strategy is best, all simulated trials were classified in terms of which navigation scheme resulted in the best miss distance. Additionally, a simple metric to characterize the winds error was needed. This strategy was intended to be as simple as possible so choice of a wind characterizing metric is an important design choice. The prevailing wind direction and distance for the waypoint wind measurement are subtracted from the wind direction and distance for the drop zone wind measurement. Additionally the difference in the time of day at which each measurement was collected are recorded.

In this way, the classifier does not rely on complicated measured of the wind which may not be available shortly before a drop. For the sake of building the classifier, the entire wind trajectory is known a priori but using such a simple metric means that the classifier could potentially be applied by relying on a simple measurement of the wind direction and distance such as dropping wind streamers or relying on the pilot's discretion.

A logistic classifier was built of the form shown in Eq. (4.9). Values for the parameters as well as explanations of the regressors are given in Table 6.

$$P = \frac{e^{\beta_1 X_1 + \beta_2 X_2 + \beta_3 X_3 + \beta_4 X_1 X_3 + \beta_5 X_2 X_3}}{1 + e^{\beta_1 X_1 + \beta_2 X_2 + \beta_3 X_3 + \beta_4 X_1 X_3 + \beta_5 X_2 X_3}} \tag{4.9}$$

Table 6: Logistic classifier coefficient values and regressor description

| **Coefficient** | **Value** |
|---|---|
| $\beta_0$ | 0.74 |
| $\beta_1$ | 0.058 |
| $\beta_2$ | 0.000064 |
| $\beta_3$ | 1.3 |
| $\beta_4$ | 0.047 |
| $\beta_5$ | 0.00062 |
| **Regressor** | **Description** |
| $X_1$ | difference in time between wind measurements |
| $X_2$ | difference in overall distance between wind measurements |
| $X_3$ | difference in overall direction between wind measurements |

The output of the logistic regression model is the probability that the waypoint navigation strategy will result in a lower miss distance than the point-toward-target scheme for a given pair of waypoint and dropzone wind files. If the predicted probability is above $50\,\%$ then the waypoint navigation scheme will be used. Otherwise the point-toward-target navigation scheme should be used. In order to build the classifier, the simulated experiments are divided into a training set and a test set according to the validation set approach. Since so much data is available in this case, a $25\,\%$ $75\,\%$ split is used. Model error is reported in terms of miss-classification. That is, the training and test error are given as a percentage which represents the portion of trials for which the wrong navigation technique is chosen by the model.

## 4.2 Results

In the following section, results from outdoor flight testing are first presented. Next results from the simulated experiments are presented. The results of a basic experiment which further demonstrates the fidelity of the simulation environment when compared to the recorded outdoor flight test data is presented. Next a more sophisticated experiment is conducted which generates a large number of simulated drops with varying characteristics in order to characterize the navigation schemes in terms of varying levels of uncertainty in drop location and drop zone winds. A simple logistic classifier is demonstrated which offers improved impact point accuracy using a rudimentary measurement of the difference in the waypoint and the drop zone winds.

### 4.2.1 Flight Test Results

Four separate outdoor flight test events were conducted in order to characterize the navigation capabilities of SnowflakeX. Testing was conducted by UMKC personnel using large UAV at Camp Roberts CA with drop altitudes ranging from $1600\,\mathrm{ft}$ to $5000\,\mathrm{ft}$ AGL. Additional testing was performed with support from staff at Yuma Proving Ground from a UH-60 Blackhawk Helicopter at Yuma Proving Ground with altitudes from $4000\,\mathrm{ft}$ to $6000\,\mathrm{ft}$. An image from this test event is shown in Figure 20.

Additional testing was conducted at Eloy AZ with support from Natick and Natick contractors from a Short Brothers SC.7 Skyvan with altitudes from $\mathrm{ft}$ to $250\mathrm{ft}$. Overall results and results by test event are shown in Table 7. The vast majority of drops conducted during test events used the point-toward-target navigation strategy but a handful

Figure 20: UH-60 Blackhawk helicopter takes off at Yuma Proving Ground

of waypoint navigation drops are included in the results as well.

Table 7: Outdoor flight test results

| **Event** | **Strategy** | **CEP** ft |
|---|---|---|
| Overall | Combined | 211 |
| Camp Roberts, CA | Combined | 225 |
| Camp Roberts, CA | Waypoint navigation | 45 |
| Camp Roberts, CA | Point-toward-target | 400 |
| Yuma Proving Ground | Point-toward-target | 8 |
| Eloy, AZ | Point-toward-target | 320 |

### 4.2.2 Simulation using Perfect CARP and Perfect Wind Estimate

An experiment was conducted to study the navigation scheme performance when the wind conditions in the drop zone are known without error. For this experiment, the same wind file used to generate the waypoints is also used to represent the winds in the drop zone during the simulation. In this way there is a perfect correlation between

the wind forecast and the winds encountered during the simulation. This experiment provides some useful data for characterizing the navigation performance and also affords an additional opportunity to evaluate the simulation performance.

Since the winds are known without error, the results of this experiment can be analyzed to determine if the generated waypoints actually reflect a ballistic trajectory. The miss distance results for the waypoint navigation strategy should be consistently very low. The results indicate that the ballistic trajectory is reasonable since the waypoint navigation scheme results in a very low CEP as shown in Figure 21.

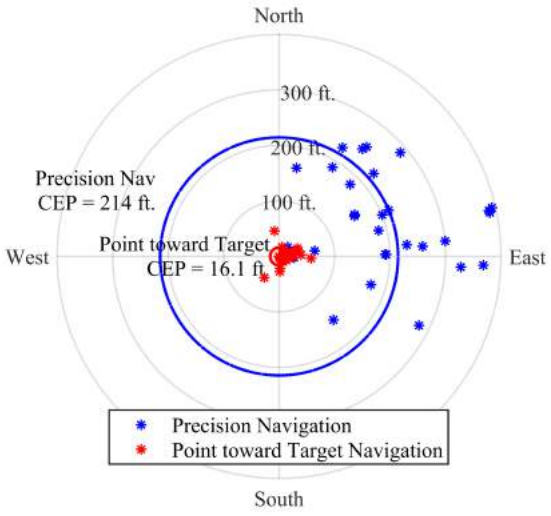


Figure 21: Comparison of landing location accuracy for different navigation schemes

### 4.2.3 Simulation Results

The ground tracks for one data set used in the experiment is shown in Figure 22. It can be seen that the point-toward-target navigation fails to account for the wind blowing

Table 8: Simulation results

| **Strategy** | **Condition** | **CEP** ft |
|---|---|---|
| Point-toward-target | winds known perfectly | 220 |
| Point-toward-target | unknown winds | 300 |
| Point-toward-target | all | 280 |
| Waypoint navigation | winds known perfectly | 16 |
| Waypoint navigation | unknown winds | 440 |
| Waypoint navigation | all | 390 |
| Both (combined) | unknown winds | 492 |
| Mixed (chosen by logistic model) | unknown winds | 264 |

toward the east and thus overshoots the target landing location and afterward cannot penetrate the wind to get back toward the target. This is why the point-toward-target navigation typically has a lower impact point accuracy compared to the waypoint navigation. Failure to account for impenetrable winds near the ground mean that the point-toward-target passes over the waypoint and does not have sufficient authority to return to the desired impact point.

Though the miss distance is better for the waypoint navigation technique, there are distinct disadvantages to this approach. Examining Figure 23 it can be seen that the desired yaw angle becomes erratic when the simulated system draws close to and overtakes a waypoint. Although, the simulated system yaw is filtered according to the system dynamics, there is still oscillation present in the simulated heading. This oscillation effectively wastes the already limited glide capability of the system. Conversely, thought the point-toward-target navigation scheme results in a larger miss distance, the desired heading is stable and thus results in a trajectory which uses the GR of the system more effectively and is more efficient in terms of controller actuation.

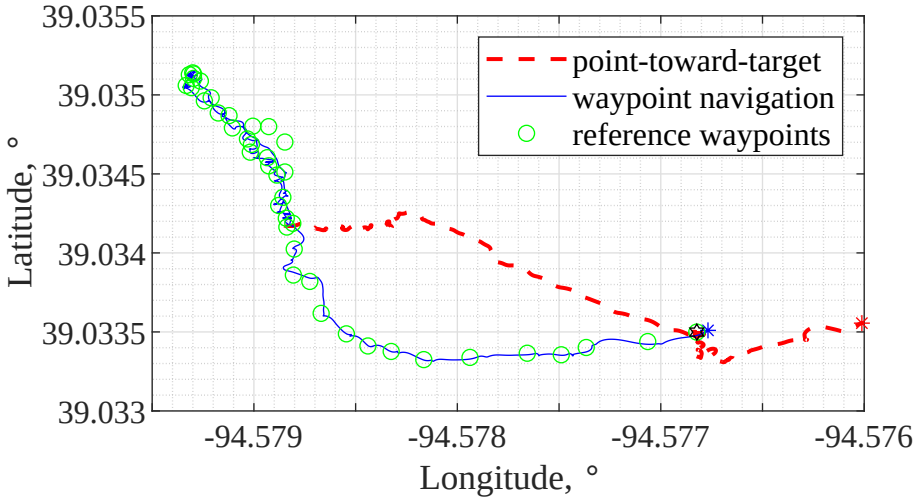


Figure 22: Comparison of ground track for different navigation schemes

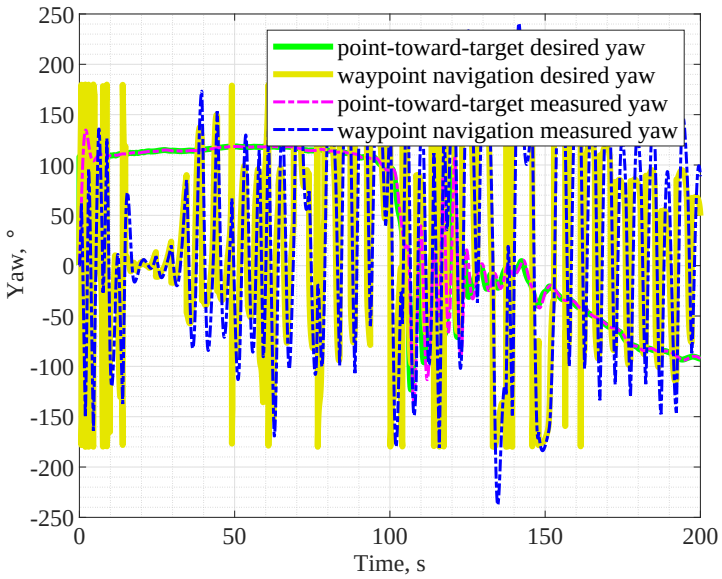


Figure 23: Comparison of yaw and desired yaw for different navigation schemes

The ground tracks in Figure 24 come from a single simulated trial where the waypoint and drop zone winds are the same. This particular trial is here representing a particularly interesting ground track. The green waypoints representing the ballistic trajectory actually start in a north-north-west direction then double back along approximately the same path. This ground track is generated based on winds which turn a full $180^\circ$ during the descent. This trial results in a particularly poor miss distance for the point-toward-target navigation scheme. It can be seen that the point-toward-target arrives at a cusp point near the desired impact point before being blown eastward by the strong, unfavorable wind near the ground. In contrast, the waypoint trajectory accounts for the strong wind near the ground by steering well to the east of the impact point.

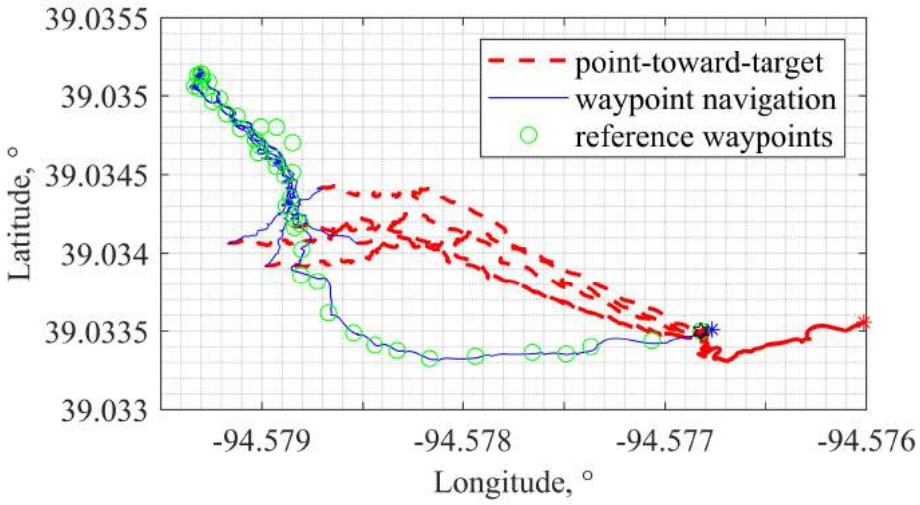


Figure 24: Comparison of ground track for different navigation schemes using imperfect CARP and erroneous wind prediction

### 4.2.4 Navigation Scheme Comparison for Imperfect CARP and Erroneous Wind Prediction

For the next simulated experiment, each wind track was first classified according to the maximum altitude recorded. Each wind track was used to generate a set of waypoints and a CARP but instead of using that same wind file to propagate the effect of the wind in the simulation, all other recorded wind files with an altitude equal to or greater than the original file was used. This generated over 450 combinations out of more than 45 recorded wind files.

A ground track plot for a representative simulated trial is shown in Figure 25. This plot provides a good graphical demonstration of the primary reason why the SnowflakeX system has difficulty arriving at the desired impact point when the winds are not know perfectly. In this case, the point-toward-target outperforms the waypoint navigation strategy slightly. Both navigation schemes fail due to a CARP which is approximately twice as far away as would be required to land close the impact point. In this case, no amount of navigation could improve the impact point accuracy substantially. The system simply does not have enough glide control authority to make up for the poor drop location.

The ground track plot shown in Figure 26 is a good representation of under what conditions the point-toward-target navigation scheme outperforms the waypoint navigation in terms of miss distance. In this case the waypoint winds and the drop zone wind measurements are not the same. Despite the wind measurements being different, they are not very far apart in terms of overall direction and distance. This highlights one of the most important disadvantages with the waypoint navigation scheme. Since the waypoints

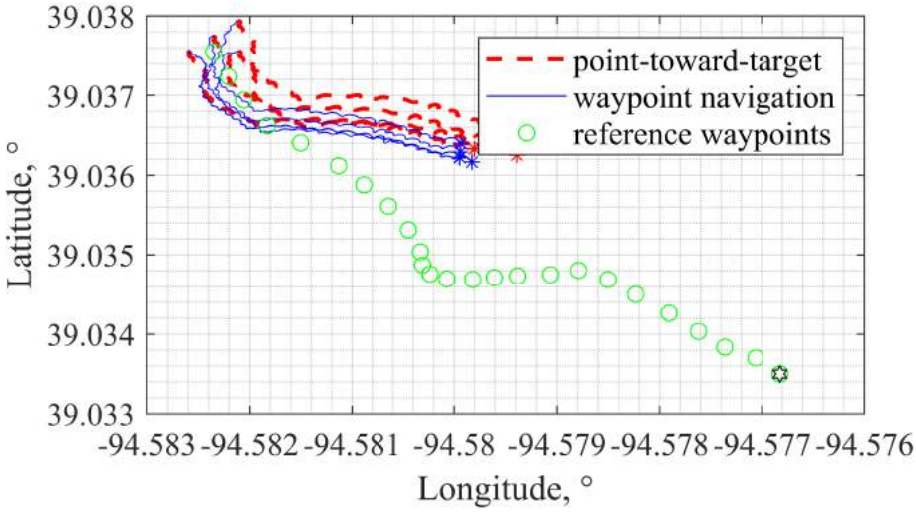


Figure 25: Ground track for representative drop with different waypoint and drop zone wind measurements

can be attained by the waypoint navigation scheme, even though they do not provide the true ballistic trajectory to the desired impact point, the waypoint navigation scheme wastes energy following the reference trajectory.

In the case of matched waypoint wind and drop zone wind measurements, the wasted energy and spoiled glide works in the favor the waypoint navigation scheme because it approximates an additional degree of freedom of control in that the system can get rid of excess distance which might otherwise be traveled in the direction of the system heading. In this case; however, the wasted glide negatively impact the miss distance. While the waypoint trajectory is foolishly tracking an imperfect trajectory, the point-toward-target strategy is making a much more efficient use of the limited translational authority to arrive very close to the desired impact point.

It is reasonable to suggest that the point-toward-target strategy outperforms the

waypoint trajectory when the wind measurements are different enough to disrupt the ballistic trajectory but not to substantially disrupt the CARP. When the systems are dropped from approximately the correct CARP, the glide which the waypoint strategy wastes is a detriment to landing location accuracy. Conversely, the extending glide capability of the more efficient (in this case) point-toward-target scheme allows the point-toward-target strategy to arrive very close to the desired impact point.

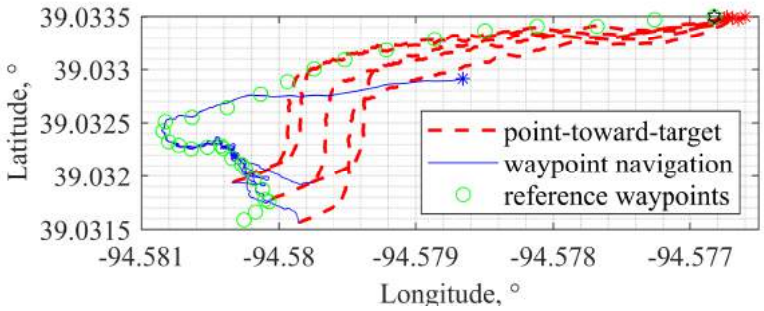


Figure 26: Ground track for representative drop with different waypoint and drop zone wind measurements

### 4.3 Navigation Experiment Conclusions

The SnowflakeX parachute system was previously proven to be capable of heading control via asymmetric deflection of the canopy by a single actuator. A controller was developed in order to stabilizing the system heading. An investigation was conducted to study the performance of different navigation potential navigation schemes to be used on SnowflakeX.

Use of the waypoint navigation scheme results in improved impact point accuracy when the winds in the drop zone are known perfectly or with a small amount of error.

When a measurement of winds in the drop zone is either not available or available only for conditions which are far away temporally or spatially, then the point-toward-target navigation results in improved impact point accuracy. A simple classifier is developed which is able to predict which strategy should be used for a given drop based on a very simple measurement of the current winds in the drop zone.

This work demonstrates the precision capabilities of the SnowflakeX system. Additionally, this work provides a groundwork for the development of more advanced navigation strategies including those capable of incorporating the wind measurement and planning a trajectory adaptively during descent.

# CHAPTER 5

# CONCLUSIONS

This work has detailed the advances made in the development of a low-cost precision guided parachute which makes use of a single actuator in order to steer an inexpensive cruciform canopy called SnowflakeX. The system serves as a solution to the precision guided airdrop problem which offers improved impact point accuracy compared to unguided ballistic systems yet is more cost effective than other options such as parafoil based solutions. The developed system is timely because, in the meantime, the US military uses low-cost, low-accuracy unguided ballistic parachute drops which leave cargo scattered across the landscape and leave aircraft vulnerable to small arms fire.

The concept behind the system is to approach the precision airdrop problem from a new angle. Rather than designing a parachute and payload system from scratch to meet impact point accuracy requirements, a simple canopy which already exists is enhanced using clever engineering design to allow precision navigation to be realized with minimal hardware development. The experimental groundwork laid out in this work is easily adapted to study other simple parachute steering concepts quickly and efficiently in a vertical wind tunnel. In this way, any type of parachute, possibly existing parachutes which were previously manufactured for purely unguided drops, might be investigated as potential precision navigation platforms in the same way the steerable cruciform system was developed.

The persistent point-to-target and waypoint navigation strategies have been used to demonstrate the precision navigation potential of the SnowflakeX system. These same techniques could be applied to any other system including those for which a controller is developed at the vertical wind tunnel. The outdoor flight test results demonstrate the viability of the SnowflakeX system as well as the viability of the specific navigation scheme being used. Additionally, the implications of these experimental results are that a wide array of unique canopies could potentially be tested using the same methodologies.

A simulation was developed for the SnowflakeX system using data obtained from the VST experiments. This simulation proved to be highly useful in characterizing the performance of different navigation schemes for SnowflakeX. A comparison between simulation results and results obtained during outdoor flight test indicates that the simulation closely matches reality. The simplicity of the simulation as well as the ease of developing the simulation using only VST experimental data means that this technique could be easily applied to other parachute systems with ease.

Ultimately, the contribution of this work is to establish framework which can be used to screen out potential precision guided airdrop solutions with a minimum investment of time and capital. The development of the SnowflakeX system serves as the first prototype of this method of development. That is, a new parachute system is designed, then tested in the vertical spin tunnel, then evaluated in limited flight testing and finally the navigation performance is evaluated extensively using a simulation. All of this development is done at a fraction of the cost and time required for the development of a traditional parachute system. Applying this methodology to other parachute designs

could delivery a whole family of precision guided airdrop solutions offering different characteristics which can be chosen based on specific operation needs. For example, the US military already makes use of a cruciform canopy called the T-11 for unguided drops which is not altogether unlike the SnowflakeX parachute. If the T-11 or any one of countless other inexpensive unguided canopies could be tested in the VST and demonstrated to be capable of precision navigation, then a mission-ready system could be developed based on that preliminary knowledge. Ultimately, systems like SnowflakeX aim to make more options and better options available to planners of re-supply missions which could lead to more accurate airdrops, less lost cargo and fewer bullet riddled aircraft.

## 5.1 Future Work

The future development of SnowflakeX involves the development of advanced trajectory planning and tracking algorithms. Reliance on a wind estimate is the continual thorn-in-the -side of parachute researchers. The impact point accuracy of all systems, including high glide and high offset capable parafoils is dependent on the accuracy of the wind estimate in the drop zone. The wind is notoriously difficult to predict and various techniques have been proposed to develop better wind estimation techniques.

The navigation scheme envisioned for SnowflakeX, will use previous knowledge of the winds in the drop zone (whether good or bad) to generate a ballistic trajectory during flight. Because the trajectory will be re-planned in flight, an estimate of the quality of the a-priori wind estimate can be obtained by compared the expected versus the actual trajectory during flight. The navigation scheme can then make decisions on the best

trajectory going forward based on the measured quality of the wind estimate.

Model predictive control (MPC) has been demonstrate as a trajectory planner on parfoil systems previously [43, 45]. Thus MPC provides a good starting point for the design of an advanced, adaptive trajectory planner.

The future of the methodologies laid out in this thesis is to employ the efficient experimental techniques to various unconventional or non-traditional guided parachute designs. Similar outdoor flight tests to those presented here could be conducted to further vet the precision navigation potential of such systems. Specifically, UMKC is currently procuring a traditionally unguided parachute from the U.S. Army Natick Soldier Research Development and Engineering Center in order to attempt to develop a stabilizing controller for the system. The unguided parachute itself was designed as part of a low-cost parachute research project and provides the perfect test case for the experimental methodology laid out in this thesis.

# APPENDIX A

## UNMANNED AERIAL SYSTEMS AND PARACHUTE RELEASE MECHANISMS

During the development of SnowflakeX two different unmanned aerial systems (UAS) were vetted and two different parachute release mechanisms were developed. The first aircraft used is a Matrice 600 which is made by DJI. This system is fully developed and ready to fly as provided. The A3 flight controller on which the M600 controller is based is incredibly robust. Additionally, the LightBridge2 system which transmits the high definition video feed from the drone along with the proprietary video receiver/radio transmitter is the most easy to use and dependable system available on the market today. The ability to use an iPad as a ground station and video viewer is a distinct advantage to using the DJI systems which is not easily available on other platforms. During outdoor flight tests, the DJI system completed dozens of autonomous landings. This capability allowed more drops to be conducted as the pilot in command could perform other tasks while monitoring the autonomous landing which would not be possible if the system was being flown manually.

As developed as the DJI system is, there is still no commercial solution for releasing a parachute from the UAS which meets all of the requirements for this project. Prior outdoor flight tests made use of a mechanism built around a payload mounting shoe which was designed to work with the Arcturus T20 fixed wing UAS. This mechanism was adapted to the multi-rotor M600 which was being used by UMKC at the time. However,

this shoe itself and the implementation of the release mechanism was sub-optimal. The design of the release mechanism was well suited to drop being conducted with non-zero forward velocity. For safety purposes, multi-rotor UAS drops are typically conducted with the aircraft hovering in place. Minimizing the forward velocity reduces the likelihood that the parachute or rigging lines could become entangled in one of the UAS rotors. Therefore, the design of the drop shoes tended to induce a rotation motion of the payload during release. Additionally, the mechanism itself was unreliable due to tolerance stack-up and excessive friction in the mechanical pull-pin release.

Figure 27: DJI M600 with magnetic parachute release system

A new mechanism was designed during the summer of 2017. This new mechanism sought to address the shortcomings of the pull-pin, shoe drop which was being used previously. Specifically the drop system needed to enable easy loading of the parachute and

payload on the UAS and needed to suffer from fewer failure-to-deploy events. The solution proposed consisted of an electromagnet powered by the M600 auxiliary power which could be switched on and off via the radio transmitter. The payload then only needed to have some kind of ferrous plate or block attached to it and it could easily loaded onto the UAS when the system was armed. With the exception of two drops, this system operated without any failure-to-deploy events in more than 100 drops at Camp Roberts, CA. The root cause of the failures was not related to the magnet drop but rather to an improperly trimmed bolt which was catching on parachute rigging lines during deployment.

Figure 28: Perfect parachute deployment from M600 UAS with magnetic payload release

The electromagnetic release mechanism had the desirable fail-safe behavior in the event of full or partial loss of power to the UAS. In the event of a power anomaly, the parachute and payload would be automatically jettisoned when the electromagnet ceased

to be energized. This left the UAS itself in the nominal configuration under which built-in fail-safe behavior should function properly and if not then pilot intervention is more straightforward under the nominal flight configuration. In order to simplify the overall system configuration, the payload was adapted to use a reed switch which would be triggered by the same electromagnet used for the mechanical dropping of the parachute in order to arm the system at the same instant the parachute was released. Use of the reed switch worked reliably for UAS drops but this method of arming became an issue during the transition to dropping from manned aircraft.

While the universality of the electromagnetic in terms of being able to lift any ferrous object within the weight limits was an advantage during the UAS drops, this same concept of a heavy chunk of steel attached to the payload is less popular when the aircraft in question is full-sized and piloted by humans on-board. During outdoor flight testing at Yuma Proving Ground in Yuma, AZ as well as flight testing at Eloy, AZ the SnowflakeX payloads were hand launched by personnel on-board the aircraft. Thus, there was no need for the electromagnetic drop mechanism. The however, left no way to arm the payload at the instant of the parachute drop. A fix was designed where the deployment bag was equipped with a permanent magnet which would be manually placed over the reed switch. When the parachute system is hand launched then the magnet is pulled from the payload and the system becomes armed. While conceptually simple, this technique was identified by drop personnel at Yuma and at Eloy as a potential safety hazard.

The drops in question were all conducted using static line deployments. This

means that when the payload exits the aircraft, the parachute deployment bag is still connected to a static line which is anchored inside the aircraft. After the system reaches the end of the static line, the parachute is forcefully removed from the deployment bag and inflates. After deployment is complete, the aircraft personnel tow the static line back into the aircraft to prevent the flapping deployment bag from contacting the fuselage. In the case of the UMKC drops, the deployment bag was outfitted with a heavy and potentially dangerous permanent magnet which could damage the aircraft if it was being whipped around by the wind. In both Yuma and Eloy, attempts were made to protect the magnet from contacting anything by drawing the magnet into the bag with the static line and by completely stitching the magnet into the deployment bag respectively. While no safety incidents were experienced at either event, the permanent magnets were tossed around strongly enough to become broken during flight on at least two occasions.

Following the Eloy, AZ testing event, a redesign of the deployment methodology was commissioned based on extensive suggestions from staff at both drop events. Two primary goals were identified in order to improve the safety of drops from manned aircraft as well as to ease the transition for UMKC staff from unmanned to manned aircraft drops. A system was desired which would work for both situations with an absolute minimum of modifications. The two goals were as follows:

1. Develop a drop mechanism which makes use of cordage only to affix the parachute and payload

2. Develop an arming method which is compatible with the drop mechanism and will also work with drop methodology used during drops from manned aircraft

The requirement of the mechanism to use cordage as the only means of affixing the system to the aircraft is born of the observation that parachute riggers at the Yuma and Eloy testing events are very comfortable working with cordage. Additionally, they are comfortable altering and tuning systems which are based on cordage. It seems as if everything that goes onto a larger parachute during the packing and rigging process is tied on. In fact it could be said that if it cannot be tied on, it will not be included in the drop. Following this maxim, the drop mechanism is to be designed such that it can be used directly or easily modified by parachute riggers during drops from manned aircraft.

The second requirement is a compliment to the first requirement. Arming mechanism for large scale airdrop seem to be based on some type of tie-off which is accomplished by the rigger as one of the last steps in the rigging process. An arming mechanism which uses cordage is easily understood by the parachute rigger and thus is less likely to be identified as a safety hazard. Even if the drop mechanism is found to be unsatisfactory, if the mechanism is based on something the parachute rigger understands such as tying off with cordage, then the system may be easily adapted in order to ease safety concerns.

A mechanism was developed which uses a more traditional type of parachute deployment bag and rigging along with a hot wire which can melt synthetic cordage in order to release the ties on system from the aircraft. This mechanism makes use of a pair of trapeze like bars which contain a nichrome resistance wire. When activated, the wire heats up and melts through whatever cordage is used to affix the payload. Although many configuration were tried during the development process, the final solution involved the cordage contacting the hot wire directly. This configuration resulted in a typical melt

time (how long to drop after the pilot engages the switch) of approximately $5\,\mathrm{s}$. Additionally, by using different weight synthetic cordage, this system can be adapted for larger or smaller payloads. The melt time can also be adjusted by switching to heavier or lighter cordage as long as the weight limits of the cordage itself are not violated.

Unfortunately, this system did not benefit from built-in fail-safe behavior like the magnet drop mechanism did. In the event of a total power failure, no energy would be available to melt the cordage and drop the system. This type of event was identified as extremely low probability anyway. In the more likely event that some type of flight anomaly was encountered and the pilot needed to land the system or the autopilot attempted to return the take-off area, the flight controller was programmed to enable the hot wire melter for all fail-safe events in order to leave the UAS unencumbered during an emergency.

Figure 29: Large UAS with hot wire melter payload release mechanism

At the same time the hot wire melter drop mechanism was designed, a new large

UAS system was built. This large UAS system increases the payload and maximum altitude capacity compared to the M600 which was previously used. Vetting this new system proved to be a daunting task. Whenever a new flight controller or aircraft is being investigated, it is imperative that all fail-safe behavior be thoroughly understood prior to the maiden flight. This includes fail-safe behavior for each component individually as well as the flight controller settings themselves. Before first flight, the pilot must be certain that the aircraft cannot flyaway and/or that if the aircraft does attempt to fly away that the fail-safe event will be triggered or the aircraft can be otherwise brought back to the ground.

After hours of ground tests and flight tests up to $400\,\mathrm{ft}$ AGL in Kansas City, the new large UAS was ready to be tested during a flight test event in Camp Roberts, CA. Despite hours of testing an in flight calibration anomaly was experienced and the large system crashed. The crash was related to a mishandled in-flight compass calibration which triggered a fail-safe event which ultimately caused a fly away due to the failure of the flight controller to trust the GPS. This event is mentioned here as just another reminder of hour important compass calibration is to aircraft flight and safety. In this specific case, the aircraft potentially could have been landed without damage if the pilot had taken the correct actions after the anomaly was experienced. Careful evaluation of potential failure modes and the best reaction in a given situation must be conducted before flying because there is often not sufficient time to think about the best thing to do during an emergency.

The takeaway from the crash event, is that stabilize mode is the least autonomous and therefore the most directly connected to the controls at the pilot's fingers. Given

sufficient altitude, it is often a good idea to attempt to switch the craft into stabilize mode prior to taking more extreme action. In the case of the large UAS crash, the pilot's decision to put the aircraft in the ground did lead to frame damage on the aircraft but if the UAS had flown higher, faster or farther away prior to the decisive action the damage could have been much worse.

To go with this hot wire melt system, an arm switch was developed which is not unlike a previous design used by UMKC. In the prior design a mechanical micro-switch is activated by a flexible nylon rod. The micro-switch state was highly dependent on the precise placement of the nylon rod and the switch itself. Additionally, since the switch is mechanical, repeated hard landings could break the switch or cause misalignment leading to faulty arming events. Additionally, the nylon rod was not captive on the payload and thus spare pieces were carried by staff at all times in order to arm and disarm the payload. Finally, the old arm switch was located inside the payload box so when the system failed to work, the entire case needed to be opened in order to fix the problem.

For the new arm switch, a photo-transistor was selected as the switching element in order to avoid all of the problems associated with mechanical switches. Plastic was first proposed as a material from which a light blocking component could be made onto which the photo-transistor could be installed and then a nylon rod could be installed or removed from a tight fitting cylinder in order to arm and disarm the system. Natural (white) nylon, black nylon and ABS were all used in the construction of prototype light blocking components. It was found that all three of these materials transmit too much light (infrared is used by the photo-transistor) and thus no reliable event which signified

that arming should take place could be identified. Eventually, aluminum was selected via experimentation as a material which provided sufficient light blocking properties without weighing too much to be used on the relatively lightweight payload.

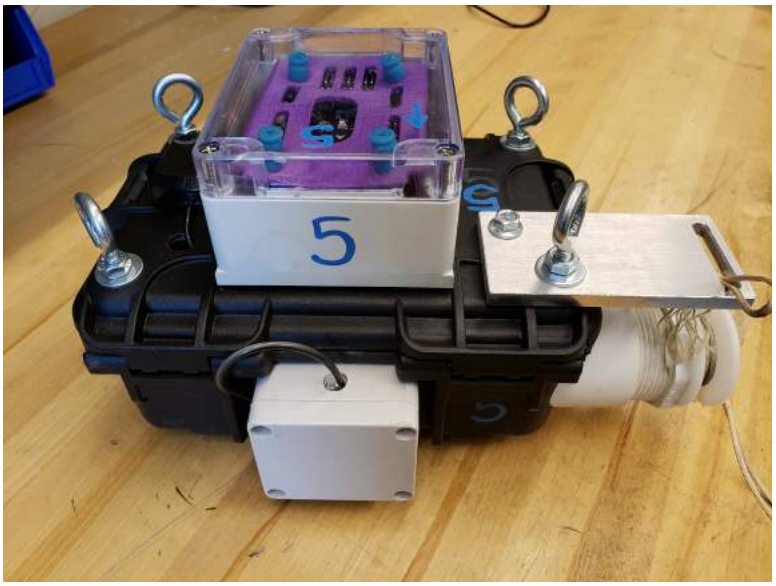


Figure 30: Redesigned payload showcasing arm switch with trigger made of black 3D printer filament

String trimmer line was used previously as the flexible nylon rod. Most string trimmer line is not perfectly round nor is the colored string trimmer line opaque. Thus, a different solution was needed in order to use the photo-transistor. It was observed that filament designed to be used in 3D printers has a consistent diameter, is available in opaque colors and is relatively flexible. Black PLA filament was selected as the flexible rod because it was already on hand. This filament showed promise but was also to blame for a handful of failure-to-deploy events. The light blocking component interacts with the flexible rod via a tight tolerance long and skinny hole. This hole was made to a tight tolerance in order to ensure that false arming events were not causes by errant light escaping past

the rod. In order to reduce the probability of failure-to-deploy events, this tight fitting cylinder was expanded considerably. Future designs should make use of as loose of a fit as possible in order to prevent the rod from sticking in the hole. Additionally, if material was available which was more flexible than the PLA filament but which provided the same light blocking abilities this material would be preferred to the 3D printer filament.

# APPENDIX B

## AERIAL GUIDANCE UNIT REDESIGN

During the summer of 2017, a modest redesign of the aerial guidance unit (AGU) was also undertaken with the goal of improving the repair-ability of the existing design. At the time the AGU was using dual winch servo motors which were originally designed for remote control sailboats to deflect the canopy and stabilize the canopy heading. These servo motors while possible some of the most robust servo motors available in the remote-controlled vehicle world, were robust enough to survive only a finite number of hard impacts. When these servo motors did fail, replacement was an ordeal which could take an hour or more and potentially delay further flight tests.

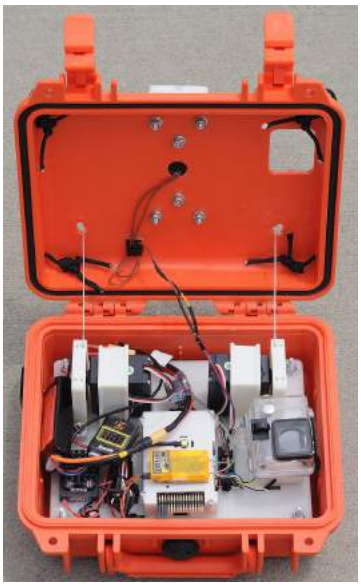

Figure 31: Payload box after redesign

The redesign itself made extensive use of plastics due to their lightweight and ease of manufacturing. A major goal of the redesign was to move the payload ballast weights inside of the AGU box in order to remove the external mounting points which made the AGU bulky and served as potential pinch and snag points for parachute rigging and for people. In order to facilitate moving the ballast weight inside the payload a false bottom was installed in the AGU under which the weights could be secured. On top of this false bottom, a host of custom designed 3D printed parts held onto the winch servo motors and other components without a minimum of fasteners. However, in order to replace most components, the false bottom first needed to be removed from the AGU so that fasteners could be accessed from below. While the servo motor mounting brackets reduced the overall system weight and made replacement of the winch spool much easier, the winch spool guides had a tendency to become entangled with the parachute control line if slack was allowed in the line such as during an off-nominal deployment or during most landings.

The redesigned system was used at Camp Roberts, CA during two test events. Additionally, the system was dropped from manned aircraft at both Yuma Proving Ground and Eloy, AZ. At both the test events involving manned aircraft, the AGU was deployed with non-zero forward velocity. At Eloy, AZ the deployment airspeed was about $120\,\mathrm{m/h}$. This serves as a testament to the robustness of a design which had obvious shortcomings. Even though the design did not look the best and even though there were areas which could have been easily improved, the sub-optimal design survived drops under various conditions.

As a direct result of suggestions from personnel at both of the manned aircraft test events, a complete redesign of the AGU was conducted during the spring of 2018. For this redesign, the following major goals were identified:

1. Use a different actuator for which spare parts can be found and which is not likely to be discontinued by the manufacturer within the next 18 months

2. Move whatever components possible to the outside of the AGU so that tasks which are most frequently required in between drops can be accomplished without opening the box

3. Redesign the arm mechanism such that cordage tied to the aircraft can be used to initiate the arm event

The first of these requirements was necessitated by ongoing problems in acquiring parts and replacements for the winch servo motors which were being used previously. The spools for these motors were easily broken and not easily replaced. Additionally, the spool were difficult to procure except as part of a package including the motor. The situation was manageable until the motors themselves became unavailable then were officially discontinued by the manufacturer. Unfortunately, no other easily obtained servo motors had specifications similar enough to be considered a drop-in replacement. To this end, the new AGU would be designed around a more robust actuator which could be expected to continue to be supported for at least a year (hopefully more) after the redesign.

At the Yuma, AZ testing event, the parachute was tied onto the top of the AGU using break-tape (cotton thread with a calibrated breaking strength which is in compliance

with a military specification). This involved tying the AGU box closed after packing which meant that no further changes could be made or problems addressed which required opening the box. In the perfect situation, the AGU would not require re-opening after packing; however, under experimental conditions and using prototype hardware, it is not uncommon to need to open a box to reset an AGU computer or to repair a servo motor or replace a servo spool. Thus the redesigned payload should include wherever possible, the ability to deal with these common problems without untying the parachute break-tape. This means that components may be moved to the outside of the box or an alternative method of tying off the parachute can be used such as providing eye hooks on the lid to tie the break-tape into.

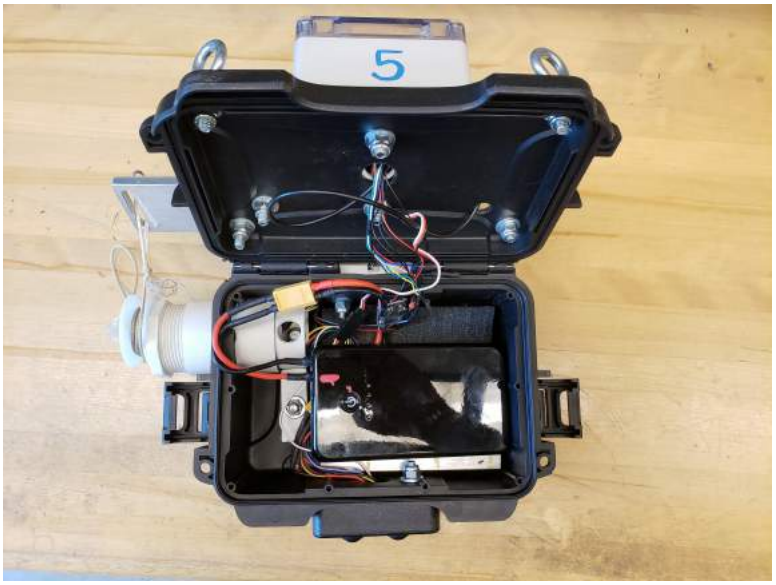


Figure 32: Wholly redesigned payload box

The last goal of the AGU design has already been discussed in the previous section. The other two design goals will be discussed here. Identifying a suitable motor

proved to be a daunting task. Motors which can be position controlled with the necessary torque and voltage ratings are simply not available within the weight constraints. Hobby-grade servo motors are not typically powerful enough; although, most are easy to power and relatively lightweight. Industrial servo motors offer easy position control with built-in feedback but can costs thousands of dollars and can weight as much as is allotted for the whole payload. Direct current (DC) gear motors are readily available but are not typically provided with native position feedback.

Ultimately, a system based on DC gear motors was selected and designed. This system makes use of commodity DC gear motors with interchangeable gear boxes which could facilitate an easy reconfiguration in the event that the existing motors were too slow or not strong enough. The gear motors in question are provided with 64 counter-per-revolution quadrature encoders already affixed to the back of the motor shaft. For the selected $30:1$ gearbox ratio, this provides a resolution of $1920$ counters per rotation of the output shaft. This resolution is comparable to the expected resolution of the servo motors which were previously used.

In order to use the quadrature encoders an Arduino program was written to decode the rising and falling edges of the quadrature square waves. The system needs to know the number of rotation as well as the direction of the rotations in order to increment or decrement the total number of steps. The motor drivers which were selected are not capable of decoding the quadrature encoder output into a position directly. In a solution which is better referred to as a hack, an Arduino handles the quadrature decoding then outputs an analog voltage to the motor driver which represents position. The motor controller has

an extremely easy-to-use graphical interface which is used for programming and tuning.

The use of the Arduino turned out to offer an additional advantage which likely would not have been possible if the quadrature decoding was happening on-board the motor controller. Previously, the rigging of the SnowflakeX parachute was a dance which involved setting a flag in the AGU computer which would let out the control line so that the parachute could be rigged with uniform suspension line lengths. Once all the line lengths were set to nominal, the AGU would be programmed with a different flag which would reel in the line so that the nominal length of the control lines could be established. This shortened length is responsible for the glide behavior and is also the neutral point of operation for the stabilizing controller. If the suspension line length varied due to cord stretch or knot slippage during descent, then the navigation performance would be degraded. Additionally, the only way to detect that the line lengths had changed was to go through the whole ordeal of programming and reprogramming the AGU and observing the change in line length.

The Arduino as a middle-man between the new actuator and the motor controller provided a remedy to the problem of establishing consistent control line lengths. Buttons were added to the Arduino which can increment and decrement the step counter without physically moving the motor. When the center point for the Arduino is changed relative to the physical motor, the motor controller receives and off-center signal and proceeds to drive the motor to the new correct position. This effectively allows the operator to dynamics shorten and lengthen the control line between each drop. Since there is no tedious re-programming involved, it is easy for the operator to perform a check between

each drop. Better yet, the buttons means that the operator can fix the problem as soon as it is discovered without even letting go of the parachute suspension lines.

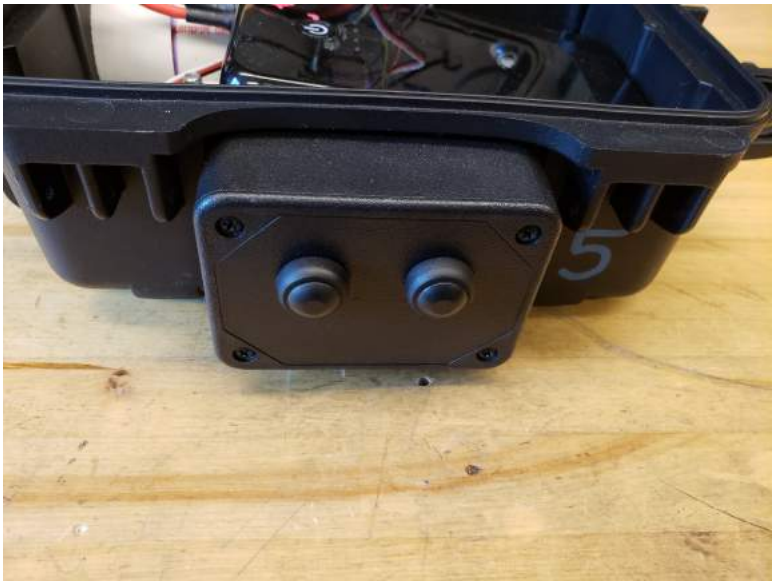

Figure 33: New payload showing jog buttons to change parachute control line lengths

In pursuit of the second goal, a smaller enclosure was selected for the redesigned AGU. This decision required that some components be moved to the outside of the box because they simply would not fit elsewhere. The AGU computer for example was moved to the top of the AGU enclosure. The AGU computer is still well protected, in fact vibration dampening balls were added to provide enhanced shock protection for the computer. Additionally, the incorporate of a computer enclosure with a transparent lid means that status lights on the AGU computer can be monitored more easily without ever opening the AGU box.

The previously described Arduino module and motor controller including the buttons was installed on the outside of the payload both because of space requirements and

because the buttons should be accessible from outside the box. Owing to well designed enclosure which includes wire strain relief and the firm positive placement of all the major electronic components, the motor controller and Arduino ensemble performed well in outdoor flight tests. In fact no components on the redesigned payload required replacement in over $40$ drops at Camp Roberts.

The arm switch which has been previously discussed is another component which was moved to the outside of the box as a result of the redesign. Apart from the issues with failure-to-deploy events, the arm switch performed as expected and was able to survive repeated hard landings. The occasional landing was abrupt enough to cause the arm switch components to become misaligned; however, the outside-the-AGU placement of the switch allowed the misalignment to be corrected very quickly.

# REFERENCE LIST


[1] Dobrokhodov, V. N., Yakimenko, O. A., and Junge, C. J., "Six-Degree-of-Freedom Model of a Controlled Circular Parachute," *Journal of Aircraft*, Vol. 40, No. 3, 2003, pp. 482–493. doi:10.2514/2.3143.

[2] Yakimenko, O. A., Dobrokhodov, V. N., Kaminer, I. I., and Dellicker, S. H., "Synthesis of Optimal Control and Flight Testing of an Autonomous Circular Parachute," *Journal of Guidance, Control, and Dynamics*, Vol. 27, No. 1, 2004, pp. 29–40. doi:10.2514/1.9282.

[3] Jorgensen, D. S., and Hickey, M. P., "The AGAS 2000 Precision Airdrop System," *Proceedings of Infotech@ Aerospace*, 2005, pp. 26–29. doi:6.2005-7072.

[4] Fields, T. D., LaCombe, J. C., and Wang, E. L., "Autonomous Guidance of a Circular Parachute Using Descent Rate Control," *Journal of Guidance, Control and Dynamics*, Vol. 35, No. 4, 2012, pp. 1367–1370. doi:10.2514/1.55919.

[5] Fields, T. D., "Evaluation of Control Line Reefing Systems for Circular Parachutes," *Journal of Aircraft*, Vol. 53, No. 3, 2016, pp. 855–860. doi:10.2514/1.C033524.

[6] Gerlach, A. R., and Doman, D. B., "Analytical Solution for Optimal Drogue-to-Main Parachute Transition Altitude for Precision Ballistic Airdrops," *Journal of Guidance, Control, and Dynamics*, Vol. 40, No. 2, 2016, pp. 439–452. doi:10.2514/1.G001824.

[7] Gerlach, A. R., Manyam, S. G., and Doman, D. B., "Precision Airdrop Transition Altitude Otimization via the one-in-a-set Traveling Salesman Problem," *2016 American Control Conference (ACC)*, IEEE, 2016, pp. 3498–3502. doi:10.1109/ACC.2016.7525455.

[8] Gerlach, A. R., Doman, D., Henry, M., and Patel, S., "Characterizing the Performance of Transition Altitude Optimization for High Altitude-Low Opening Ballistic Airdrop," *24th AIAA Aerodynamic Decelerator Systems Technology Conference*, AIAA, 2017. doi:10.2514/6.2017-3221.

[9] Vandermey, J. T., Doman, D. B., and Gerlach, A. R., "Release Point Determination and Dispersion Reduction for Ballistic Airdrops," *AIAA Atmospheric Flight Mechanics Conference*, AIAA, 2016. doi:10.2514/6.2016-1537.

[10] Slegers, N., and Yakimenko, O., "Terminal Guidance of Autonomous Parafoils in High Wind-to-airspeed ratios," *Proceedings of the Institution of Mechanical Engineers, Part G: Journal of Aerospace Engineering*, Vol. 225, No. 3, 2011, pp. 336–346. doi:10.1243/09544100JAERO749.

[11] Bergeron, K., Ward, M., and Costello, M., "Aerodynamic Effects of Parafoil Upper Surface Bleed Air Actuation," *AIAA Atmospheric Flight Mechanics Conference*, Vol. 4737, AIAA, 2012. doi:10.2514/6.2012-4737.

[12] Bergeron, K., Seidel, J., and McLaughlin, T., "Wind Tunnel Investigations of Rigid Ram-Air Parachute Canopy Configurations," *23rd AIAA Aerodynamic Decelerator Systems Technology Conference*, Vol. 2156, AIAA, 2015. doi:10.2514/6.2015-2156.

[13] Kaminer, I., and Yakimenko, O., "Development of Control Algorithm for the Autonomous Gliding Delivery System," *Proceedings of the 17th AIAA Aerodynamic Decelerator Systems Technology Conference and Seminar*, Vol. 2116, AIAA, 2003. doi:10.2514/6.2003-2116.

[14] Scheuermann, E., Ward, M., Costello, M., Bergeron, K., and Noetscher, G., "Bleed Air Control: Towards the Complete In-Canopy System for Autonomous Aerial Delivery," *24th AIAA Aerodynamic Decelerator Systems Technology Conference*, Vol. 3883, AIAA, 2017. doi:10.2514/6.2017-3883.

[15] Yakimenko, O., Slegers, N., and Tiaden, R., "Development and Testing of the Miniature Aerial Delivery System Snowflake," *20th AIAA Aerodynamic Decelerator Systems Technology Conference and Seminar*, Vol. 2980, AIAA, 2009. doi:10.2514/6.2009-2980.

[16] Yakimenko, O. A., and Slegers, N. J., "Using Direct Methods for Terminal Guidance of Autonomous Aerial Delivery Systems," *Control Conference (ECC), 2009 European*, IEEE, 2009, pp. 2372–2377. URL https://calhoun.nps.edu/bitstream/handle/10945/35328/Yakimenko_Using_Direct_Methods_for_Terminal_Guidance_of_Autonomous_Aerial_Delivery_Systems.pdf?sequence=1.

[17] Fields, T. D., and Yakimenko, O. A., "Development of a Steerable Single-Actuator Cruciform Parachute," *Journal of Aircraft*, 2017, pp. 1–9. doi:10.2514/1.C034416.

[18] Potvin, J., Papke, J., Brighton, E., Hawthorne, T., Peek, G., and Benney, R., "Glide Performance Study of Standard and Hybrid Cruciform Parachutes," *Proceedings of the 17th AIAA Aerodynamic Decelerator Systems Technology Conference and Seminar*, Vol. 2160, AIAA, 2003. doi:10.2514/6.2003-2160.

[19] Haller, J., Fields, T., and Yakimenko, O. A., "Precision Aerial Delivery with a Steerable Cruciform Parachute," *24th AIAA Aerodynamic Decelerator Systems Technology Conference*, AIAA, 2017, p. 3539. doi:10.2514/6.2017-3539.

[20] Potvin, J., Peek, G., Brocato, B., Perschbacher, T., Kutz, R., and Benney, R., "Inflation and Glide Studies of Slider Reefed Cruciform Parachutes," *16th AIAA Aerodynamic Decelerator Systems Technology Conference and Seminar*, Vol. 2021, AIAA, 2001, pp. 194–212. doi:10.2514/6.2001-2021.

[21] of Defense. Joint Parachute Test Facility, U. S. D., "Department of Defense Joint Parachute Test Facility," Tech. rep., Joint Parachute Test Facility, Department of Defense, Mar 1968. URL http://lhldigital.lindahall.org/cdm/ref/collection/parachute/id/678.

[22] Braun, G. W., "Stability of a Whirling Gondola Suspended from a Parachute-Testing Tower," Tech. rep., Aeronautical Systems Division, Wright-Patterson Air Force Base Flight Control Lab, Jan 1953. URL http://www.dtic.mil/dtic/tr/fulltext/u2/005009.pdf.

[23] Gross, R. J., and Eckstrom, C. V., "Performance Evaluation of Parachute Canopies with Various Cloth Permeabilities," Tech. rep., Flight Accessories Laboratory, Aeronautical Systems Division, Air Force Systems Command, 6 1962. URL http://www.dtic.mil/get-tr-doc/pdf?AD=AD0284395.

[24] Barton, R. L., "Scale Factors for Parachute Opening," Tech. rep., NASA, Sep 1967. URL https://ntrs.nasa.gov/search.jsp?R=19670026449.

[25] Maire, R., and Wells, R. D., "Engineering Evaluation of Age Life Extension, T-10

Harnesses, Risers and T-10 Troop Chest Reserve Parachute Canopies," Tech. rep., US Army Natick Laboratories, Mar 1972. URL http://www.dtic.mil/get-tr-doc/pdf?AD=AD0742668.

[26] Wells, R. D., Devarakonda, V. K., and Mahar, M. E., "Engineering Evaluation of Age Life Extension, T-10 Troop Main Parachute," Tech. rep., US Army Natick Laboratories, Mar 1974. URL http://www.dtic.mil/docs/citations/AD0779956.

[27] von Bengtson, K., "Introducing Space Test Center Lindoe," , Feb 2012. URL https://www.wired.com/2012/02/introducing-space-test-center-lindoe/.

[28] von Bengtson, K., "Do Not Be Afraid of the DIY Space Parachute - It Might Just Work," , Mar 2012. URL https://www.wired.com/2012/03/do-not-be-afraid-of-the-diy-space-parachute-it-might-just-work/.

[29] Lorenz, R. D., Dooley, J. M., and Brock, K., "Parachute Drop-Tests and Attitude Measurements of a Scale-Model Huygens Probe from Model Aircraft," *Proceedings of the International Planetary Probe Workshop IPPW-3 Athens, Greece*, Vol. 3, NASA, 2005. URL https://solarsystem.nasa.gov/docs/18_lorentz.pdf.

[30] Naval Air Warfare Center Weapons Division Public Affairs, "New Method of Testing Parachutes Developed at China Lake," , Nov 2013. URL http://www.navair.navy.mil/index.cfm?fuseaction=home.NAVAIRNewsStory&id=5497.

[31] von Bengtson, K., "DIY Space Capsule Wind Tunnel Testing - One More Time Please," , Mar 2013. URL https://www.wired.com/2013/03/diy-space-capsule-wind-tunnel-testing-one-more-time-please/.

[32] Hillje, E., and Igoe, W., "Transonic Dynamic Stability Characteristics of Several Models of Project Mercury Capsule Configurations," Tech. rep., NASA, Aug 1961. URL https://ntrs.nasa.gov/search.jsp?R=19660027825.

[33] Ghoreyshi, M., Bergeron, K., Seidel, J., Jirásek, A., Lofthouse, A. J., and Cummings, R. M., "Prediction of Aerodynamic Characteristics of Ram-Air Parachutes," *Journal of Aircraft*, Vol. 53, No. 6, 2016, pp. 1802–1820. doi:10.2514/1.C033763.

[34] Fremaux, C. M., "Spin-tunnel Investigation of a 1/28-Scale Model of the NASA F-18 High Alpha Research Vehicle (HARV) with and without Vertical Tails," Tech. rep., NASA, Apr 1997. URL https://ntrs.nasa.gov/search.jsp?R=19970019598.

[35] Neilhouse, A. I., Klinar, W. J., and Scher, S. H., "Status of Spin Research for Recent Airplane Designs," Tech. rep., National Advisory Committee for Aeronautics, Apr 1957. URL https://ntrs.nasa.gov/search.jsp?R=19930089716.

[36] Kaminer, I., Pascoal, A., Hallberg, E., and Silvestre, C., "Trajectory Tracking for Autonomous Vehicles: An Integrated Approach to Guidance and Control," *Journal of Guidance, Control, and Dynamics*, Vol. 21, No. 1, 1998, pp. 29–38. doi:10.2514/2.4229.

[37] Kaminer, I., Yakimenko, O., Dobrokhodov, V., Pascoal, A., Hovakimyan, N., Patel, V., Cao, C., and Young, A., "Coordinated Path Following for Time-Critical Missions of Multiple UAVs via L1 Adaptive Output Feedback Controllers," *AIAA Guidance, Navigation and Control Conference and Exhibit*, AIAA, 2007, p. 6409. doi:10.2514/6.2007-6409.

[38] Kaminer, I., Pascoal, A., Xargay, E., Hovakimyan, N., Cao, C., and Dobrokhodov, V., "Path Following for Small Unmanned Aerial Vehicles Using L1 Adaptive Augmentation of Commercial Autopilots," *Journal of guidance, control, and dynamics*, Vol. 33, No. 2, 2010, pp. 550–564. doi:10.2514/1.42056.

[39] Oh, S.-R., and Sun, J., "Path Following of Underactuated Marine Surface Vessels Using Line-of-Sight Based Model Predictive Control," *Ocean Engineering*, Vol. 37, No. 2-3, 2010, pp. 289–295. doi:10.1016/j.oceaneng.2009.10.004.

[40] Richards, A., and How, J. P., "Model Predictive Control of Vehicle Maneuvers with Guaranteed Completion Time and Robust Feasibility," *American Control Conference, 2003. Proceedings of the 2003*, Vol. 5, IEEE, 2003, pp. 4034–4040. doi:10.1109/ACC.2003.1240467.

[41] Howard, T. M., Green, C. J., and Kelly, A., "Receding Horizon Model-Predictive Control for Mobile Robot Navigation of Intricate Paths," *Field and Service Robotics*, Springer, 2010, pp. 69–78. doi:10.1007/978-3-642-13408-1_7.

[42] Castillo, C., Moreno, W., and Valavanis, K., "Unmanned Helicopter Waypoint Trajectory Tracking using Model Predictive Control," *Control & Automation, 2007. MED'07. Mediterranean Conference on*, IEEE, 2007, pp. 1–8. doi:10.1109/MED.2007.4433726.

[43] Slegers, N., and Costello, M., "Model Predictive Control of a Parafoil and Payload System," *Journal of Guidance, Control, and Dynamics*, Vol. 28, No. 4, 2005, pp. 816–821. doi:10.2514/1.12251.

[44] Alexis, K., Nikolakopoulos, G., and Tzes, A., "Switching Mode Predictive Attitude Control for a Quadrotor Helicopter Subject to Atmospheric Disturbances," *Control Engineering Practice*, Vol. 19, No. 10, 2011, pp. 1195–1207.

[45] Slegers, N., Kyle, J., and Costello, M., "Nonlinear Model Predictive Control Technique for Unmanned Air Vehicles," *Journal of guidance, control, and dynamics*, Vol. 29, No. 5, 2006, pp. 1179–1188. doi:10.2514/1.21531.

[46] Bouffard, P., Aswani, A., and Tomlin, C., "Learning-Based Model Predictive Control on a Quadrotor: Onboard Implementation and Experimental Results," *Robotics and Automation (ICRA), 2012 IEEE International Conference on*, IEEE, 2012, pp. 279–284. doi:10.1109/ICRA.2012.6225035.

[47] Gursoy, G., Prach, A., and Yavrucuk, I., "Design of a Waypoint Tracking Control Algorithm for Parachute-Payload Systems," 2013, pp. 343–359.

[48] Zhang, L., Gao, H., Chen, Z., Sun, Q., and Zhang, X., "Multi-Objective Global Optimal Parafoil Homing Trajectory Optimization via Gauss Pseudospectral Method," *Nonlinear dynamics*, Vol. 72, No. 1-2, 2013, pp. 1–8. doi:10.1007/s11071-012-0586-9.

[49] Luders, B. D., Sugel, I., and How, J. P., "Robust Trajectory Planning for Autonomous Parafoils Under Wind Uncertainty," *AIAA Infotech@ Aerospace (I@ A) Conference*, AIAA, 2013, p. 4584. doi:10.2514/6.2013-4584.

[50] Slegers, N., Beyer, E., and Costello, M., "Use of Variable Incidence Angle for Glide Slope Control of Autonomous Parafoils," *Journal of Guidance, Control, and Dynamics*, Vol. 31, No. 3, 2008, pp. 585–596. doi:10.2514/1.32099.

[51] NASA, "NASA 20ft. Vertical Spin Tunnel," Tech. rep., NASA, 2016. URL https://crgis.ndc.nasa.gov/historic/20-Foot_Spin_Tunnel, accessed: 2018-02-05.

[52] O H Madgwick, S., "An efficient orientation filter for inertial and inertial/magnetic sensor arrays," Tech. rep., Report x-io and University of Bristol (UK), 2010.

# VITA

Shawn Malachy Herrington was born on December 31, 1990 in Kansas City, MO. He attended St. Peter's grade school in Kansas City and then attended Bishop Miege High School in Roeland Park, KS and graduated in 2009. In 2017, he graduated Summa Cum Laude from the University of Missouri Kansas City with a Bachelor's of Science Degree in Mechanical Engineering. Since graduation, he has worked as a graduate research assistance under Dr. Travis Fields in the Parachute and Aerial Vehicle Systems laboratory. During this time, he also worked as a Teacher's Assistant for the Mechatronics Systems Design Course at UMKC. Shawn's research has focused on the development of a stabilizing controller and comparative investigation into trajectory planning and tracking controllers for an affordable guided parachute drop system. After graduation Shawn plans to continue his education at UMKC.